High-resolution spectroscopy and global analysis of CF4 rovibrational bands to model its atmospheric absorption

M. Carlos, O. Gruson, C. Richard, Vincent Boudon, M. Rotger, X. Thomas, C. Maul, C. Sydow, A. Domanskaya, Robert Georges, et al.

Highlights

- Global analysis of many rovibrational bands of CF4.
- This allows to simulate hot bands in the strongly absorbing 3 region.
- The results allow to model 92 % of the atmospheric absorption of this greenhouse gas.
- They have been used for spectroscopic database updates, including HITRAN2016.

High-resolution spectroscopy and global analysis of CF_4 rovibrational bands to model its atmospheric absorption

M. Carlos[a,b,c], O. Gruson[a], C. Richard[a], V. Boudon[a], M. Rotger[d], X. Thomas[d], C. Maul[e], C. Sydow[e], A. Domanskaya[f,g], R. Georges[h], P. Soulard[i,j], O. Pirali[k,l], M. Goubet[m], P. Asselin[i,j] and T. R. Huet[m]

[a] *Laboratoire Interdisciplinaire Carnot de Bourgogne, UMR 6303 CNRS - Université Bourgogne Franche-Comté, 9 Av. A. Savary, BP 47870, F-21078 Dijon Cedex, France.*

[b] *Université de Toulouse, UPS-OMP, Institut de Recherche en Astrophysique et Planétologie, Toulouse, France*

[c] *CNRS, IRAP, 9 Av. Colonel Roche, BP 44346, F-31028, Toulouse Cedex 4, France*

[d] *GSMA, UMR CNRS 7331, Université de Reims Champagne Ardenne, Moulin de la Housse B.P. 1039, F-51687, Cedex Reims, France*

[e] *Institut für Physikalische und Theoretische Chemie, Technische Universität Braunschweig, Gaußstr. 17, 38106 Braunschweig, Germany*

[f] *Saint Petersburg State University, 7/9 Universitetskaya Nab., 199034, Saint Petersburg, Russian Federation*

[g] *Current address: Physikalisch-Technische Bundesanstalt (PTB), Bundesallee 100, D-38116 Braunschweig, Germany*

[h] *Institut de Physique de Rennes, UMR 6251, Campus de Beaulieu, Université de Rennes 1/CNRS, F-35042 Rennes Cedex, France*

[i] *Sorbonne Universités, UPMC Univ Paris 06, UMR 8233, MONARIS, F-75005, Paris, France*

[j] *CNRS, UMR 8233, MONARIS, F-75005, Paris, France*

[k] *Ligne AILES- Synchrotron SOLEIL, L'Orme des Merisiers, F-91192 Gif-sur-Yvette Cedex, France*

[l] *Institut des Sciences Moléculaires d?Orsay (ISMO), CNRS, Univ. Paris-Sud, Université Paris-Saclay, F-91405 Orsay, France*

[m] *Univ. Lille, CNRS, UMR 8523 - PhLAM - Physique des Lasers Atomes et Molécules, F-59000 Lille, France.*

Abstract

CF_4, or tetrafluoromethane, is a chemically inert and strongly absorbing greenhouse gas, mainly of anthropogenic origin. In order to monitor and reduce its atmospheric emissions and concentration, it is thus necessary to obtain an accurate model of its infrared absorption. Such models allow opacity calculations for radiative transfer atmospheric models. In the present work, we perform a

global analysis (divided into two distinct fitting schemes) of 17 rovibrational bands of CF_4. This gives a reliable model of many of its lower rovibrational levels and allows the calculation of the infrared absorption in the strongly absorbing ν_3 region (1283 cm^{-1} / 7.8 μm), including the main hot band, namely $\nu_3 + \nu_2 - \nu_2$ as well as $\nu_3 + \nu_1 - \nu_1$; we could also extrapolate the $\nu_3 + \nu_4 - \nu_4$ absorption. This represents almost 92 % of the absorption at room temperature in this spectral region. A new accurate value of the C–F bond length is evaluated to $r_e = 1.314860(21)$ Å. The present results have been used to update the HITRAN, GEISA and TFMeCaSDa (VAMDC) databases.

Keywords: Carbon tetrafluoride, Tensorial Formalism, Spherical Top, Fourrier Transform Infrared Spectroscopy, Global fit, Line Positions and Intensities

1. Introduction

Tetrafluoromethane (CF_4), also known as Halocarbon 14, PFC-14 or R-14, is a colorless, non-toxic, non-flammable, non-corrosive gas belonging to the group of perfluorocarbons (PFCs). PFCs are extremely powerful greenhouse gases and find themselves among the longest-lived atmospheric traces gases because of their great chemical stability. CF_4 is the most abundant PFC in the stratosphere, where it has an estimated lifetime of more than 50,000 years [1, 2]. For these reasons, CF_4 is cited in the Kyoto Protocol [3, 4, 5] as a substance whose atmospheric concentration should be monitored and reduced. Infrared high spectral resolution solar occultation spectrometer measurements (Atmospheric Chemistry Experiment) led to an abundance of 70.45 ± 3.40 pptv (10^{-12} per unit volume) [6]. Part of this is of natural origin [7, 8, 9]. The main source of CF_4, however, is anthropogenic and related to aluminum refining and to semiconductor manufacturing [10]. Recent studies from the ground and from space [6, 11, 12] detailed the evolution of CF_4's atmospheric concentration.

The *in situ* detection of atmospheric CF_4 is based on infrared solar absorption spectroscopy. The very intense ν_3 vibration-rotation band around 7.8 μm was used for the first detection of CF_4 in the atmosphere from balloon-borne

observations [13]. Volumetric mixing ratio profiles of CF_4 were retrieved from satellite-borne [6, 14, 15] and balloon-borne observations [16]. The public spectroscopic databases like HITRAN [17, 18] or GEISA [19, 20], however, are not complete enough for atmospheric applications, since they completely lack hot band lines. This causes huge errors in CF_4 concentration retrievals when using these databases, as shows in Ref. [21]. The authors of this paper already pointed out that the lack of hot band lines in the databases is the main problem; thus, they used an empirical list of pseudo lines instead, which is much less flexible for simulations at any temperature.

Table 1 recalls the normal modes of this molecule. Using a simple harmonic approximation, it is easy to evaluate the population $P(v_1, v_2, v_3, v_4)$ of the different vibrational levels, as a function of temperature T [22] as:

$$P(v_1, v_2, v_3, v_4) = \frac{g_v}{Q_v(T)} e^{-\frac{1}{k_B T}(v_1\widetilde{\nu}_1 + v_2\widetilde{\nu}_2 + v_3\widetilde{\nu}_3 + v_4\widetilde{\nu}_4)}, \quad (1)$$

where g_v is the vibrational level's degeneracy and $Q_v(T)$ the vibrational partition function. This is plotted for CF_4 on Figure 1. We thus see that the sole ν_3 fundamental band, also very strong, represents less than two-thirds of the absorption intensity at 296 K. In order to obtain a correct modelling of the molecule's opacity, it is thus mandatory to model hot bands, at least the one starting from the first excited vibrational level, $v_2 = 1$ (435.38 cm^{-1}), that is the $\nu_3 + \nu_2 - \nu_2$ band.

Mode ν_i	ν_1	ν_2	ν_3	ν_4
Symmetry	A_1	E	F_2	F_2
Degeneracy	1	2	3	3
Type	Stretching	Bending	Stretching	Bending
Activity	Raman	Raman	Absorption/Raman	Absorption/Raman
$\widetilde{\nu}_i$ / cm^{-1}	909.1	435.4	1283.2	631.1

Table 1: The normal modes of vibration of CF_4. Symmetry is the mode's irreducible representation in the T_d point group. Activity is given for the fundamental band. $\widetilde{\nu}_i$ is the approximate wavenumber for $^{12}CF_4$ taken from the present study (from Tables A.6 and B.7).

To achieve this goal, it is thus necessary to know at first the lowest vibrational states (like bands with $v_2 = v_3 = 1$ in the above example). The purpose of

the present paper is to perform a global and consistent analysis of as many rovibrational transitions as possible, gathering existing and new experimental data, in order to obtain a reliable modeling of CF_4'a absorption spectrum in the ν_3 region, including the most significant hot bands. We complete here our two previous studies [23] and [24] with extensive new experimental data, strongly increasing the number of assigned lines and of studied bands.

Section 2 details the various data used, while Section 3 recalls the spherical-top model used for analysis and modeling. In Section 4, we present line assignments and effective Hamiltonian parameter fits. Line intensities are discussed in Section 5 and, finally, Section 6 presents the recent database updates concerning CF_4.

2. Experimental Details

This work gathers different data sources which are summarized in Table 2. We describe here the new spectra that have been recorded recently for this study.

It should be noticed that the uncertainty on line positions associated to high resolution Fourier Transform spectra is typically better than 0.001 cm^{-1}, while that of Raman spectra may be somewhat worse. However, knowing that we use here a huge number of lines from various sources, with different pressures, signal-to-noise ratios and apodization functions, we considered in the present study that all the line positions have a similar accuracy.

2.1. Infrared absorption data from Reims

The spectra are recorded with the Fourier Transform Spectrometer (FTS) of the GSMA laboratory already described elsewhere [25, 26]. The different characteristics of the spectra are reported in Table 2 (experimental conditions). The value of the diaphragm is 4 mm. The temperature of the cell was not stabilized, this is a 2 m-long White cell with an equivalent path length of 8.262 m. We

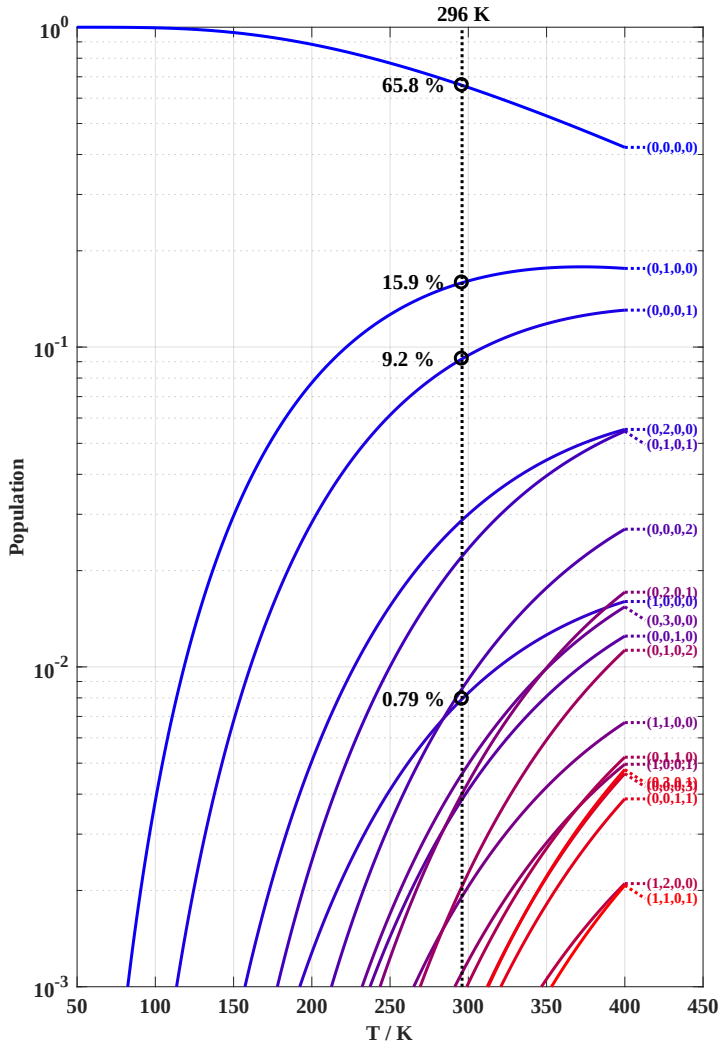

Figure 1: Population of the vibrational levels of CF_4, as a function of temperature. Values at 296 K for the four lower levels involved in the hot bands calculated in the present work (see Section 5) are indicated. On the right, vibrational levels are labelled using the vibrational quantum number quadruplet, (v_1, v_2, v_3, v_4), see Table 1 and Section 3.

use two different detectors, a photovoltaic HgCdTe (or MCT) detector cooled at 77 K for the $\nu_2 + (\nu_3/2\nu_4)$ region and an InSb detector cooled at 77 K for the $\nu_1 + (\nu_3/2\nu_4)$ region, a Globar source, and different selected optical filters.

2.2. Infrared absorption data from Braunschweig

Room temperature CF_4 spectra were recorded with a high resolution FTS (Bruker IFS120HR) using a White multiple pass absorption cell with a path length of 4 m, equipped with KBr windows. The $\nu_2 + \nu_4$ and $\nu_1 + \nu_4$ bands were recorded using slightly different experimental conditions listed hereafter and grouped in Table 2.

A liquid nitrogen cooled MCT detector and a globar source combination was systematically used for the recording of the two bands. A KBr beam splitter was used for both bands. Gas pressures were monitored with a MKS capacitance gauge. The spectral resolution was 0.003 cm^{-1}. The $\nu_1+\nu_4$ band was monitored at a gas pressure of 15 Torr (20 mbar) by co-adding 70 scans while the $\nu_2 + \nu_4$ band was recorded at a gas pressure of 11.25 Torr (15 mbar) by co-adding 200 scans.

2.3. Far infrared room temperature absorption data from SOLEIL

The far infrared room temperature data were recorded using the synchrotron radiation delivered by the AILES beamline of the synchrotron SOLEIL. The high-resolution FTS (Bruker IFS 125 HR) available on the beamline was connected to a White multiple pass optical cell to achieve an absorption path length of 150 m. The FTS was settled to its maximal resolution (0.00102 cm^{-1}) and a 6 μm thick mylar beam splitter and a bolometer equipped with an internal optical filter were used to record the 40–580 cm^{-1} spectral range. A total of 326 and 274 scans were co-added for a gas pressure of 2.6 and 18 Torr respectively.

2.4. Jet-cooled infrared absorption data from SOLEIL

The jet-cooled absorption spectrum was recorded using the Jet-AILES apparatus implemented on the AILES beamline [27]. The infrared light beam

produced by the internal Globar source of the FTS was focused through a continuous planar supersonic expansion formed by a 30 μm $\times$ 60 mm slit nozzle. A throughput of about 6 slm (standard liter per minute) of CF_4 in 20 slm of argon was regulated by appropriate Bronkhorst mass flow controllers all along the recording. The total stagnation pressure was 1530 Torr and the vacuum chamber pressure was 0.66 Torr. KBr windows were used to isolate the vacuum chamber from the FTS and the detector compartment see Ref. [27]. A combination of a KBr beam splitter, a MCT photovoltaic detector and an adapted optical filter was used to co-add 386 scans in the 900–2700 cm^{-1} spectral range, at a resolution of 0.002 cm^{-1}, and a rotational temperature of about 50 K.

2.5. THz rotational absorption data from SOLEIL

We also used newly recorded rotational lines in the $v_3 = 1$ state ($\nu_3 - \nu_3$ hot band) in the THz region (20–36 cm^{-1}). This dataset will be described in a forthcoming paper [28].

2.6. Earlier infrared absorption and Raman scattering data

We also use $\nu_3/2\nu_4$ infrared absorption and ν_1, $2\nu_2 - \nu_1$ and ν_2 stimulated Raman data taken from our previous works and described in Refs. [23] and [24], respectively.

3. Theoretical model

CF_4, just like CH_4 and other tetrahedral spherical top molecules with T_d point group symmetry at equilibrium, possesses four normal modes of vibration: one non-degenerate mode with A_1 symmetry (ν_1), one doubly-degenerate mode with E symmetry (ν_2), and two triply-degenerate modes with F_2 symmetry (ν_3 and ν_4), see Table 1. Only F_2 fundamentals are infrared active, at first approximation, but other vibrational levels can gain some absorption intensity through Coriolis and anharmonic couplings (see for instance [29, 30]).

Transitions	Type	$\widetilde{\nu}_0/\mathrm{cm}^{-1}$	Place	T/K	P/Torr	d/m	R/cm^{-1}	Reference
Spectra used for the "ν_2" fit								
$\nu_3-\nu_3$	THz	35	SOLEIL	296	100	150	0.001	[28]
ν_2	IR	435	SOLEIL	296	18	150	0.001	This work
ν_2	IR	435	IPR Rennes	296	501	970	0.02	[29]†
ν_2	Raman	435	CSIC Madrid	296	1.5	—	0.003	[24]
ν_4	IR	435	SOLEIL	296	2.6	150	0.001	This work
$\nu_2+\nu_4$	IR	1066	Braunschweig	296	11.25	4	0.003	This work
$2\nu_2$	Raman	870	CSIC Madrid	135	22.5	—	0.003	[24]
$2\nu_2$	Raman	870	CSIC Madrid	296	11.3	—	0.003	[24]
$\nu_3/2\nu_4$	IR	1283	Braunschweig	Several spectra, see Reference				[23]
$\nu_3/2\nu_4$	IR jet	1283	SOLEIL	50	—	0.06	0.002	This work
$\nu_2+(\nu_3/2\nu_4)$	IR jet	1720	SOLEIL	50	—	0.06	0.002	This work
$\nu_2+(\nu_3/2\nu_4)$	IR	1720	GSMA Reims	295	5	8.262	0.003	This work
Spectra used for the "ν_1" fit								
$\nu_1-\nu_4$	Far-IR	278	SOLEIL	296	18	150	0.001	This work
ν_1	Raman	909	CSIC Madrid	135	1.5	—	0.003	[24]
ν_1	Raman	909	CSIC Madrid	295	3.75	—	0.003	[24]
$2\nu_1-\nu_1$	Raman	906	CSIC Madrid	296	22.5	—	0.003	[24]
$\nu_1+\nu_4$	IR	1540	Braunschweig	296	15	4	0.003	This work
$\nu_1+(\nu_3/2\nu_4)$	IR jet	2186	SOLEIL	50	—	0.06	0.001	This work
$\nu_1+(\nu_3/2\nu_4)$	IR	2186	GSMA Reims	295	0.5	8.262	0.003	This work

† This spectrum was not used for the present analyses, but it is compared to a high-pressure simulation in Figure 5 below.

Table 2: Experimental spectra used for the analyses. They were recorded in different laboratories. $\widetilde{\nu}_0$ is the approximate wavenumber, T the temperature, P the pressure, d the optical path and R the spectral resolution.

3.1. Effective Hamiltonian

In this paper we use the theoretical model based on the tensorial formalism and the vibrational extrapolation concept developed by the Dijon group [31, 32]. It takes full advantage of the molecule's high symmetry. Let us just recall briefly the principles of this model which have been already detailed in Ref. [32]. Considering an XY_4 molecule such as CF_4, the vibrational levels are grouped in series of polyads named P_k with $k=0,\ldots,n$. For $k=0$, we have P_0 which is the ground state (GS). The Hamiltonian operator is written as follows:

$$\mathcal{H}=\mathcal{H}_{\{P_0\equiv GS\}}+\mathcal{H}_{\{P_1\}}+\ldots+\mathcal{H}_{\{P_k\}}+\ldots+\mathcal{H}_{\{P_{n-1}\}}+\mathcal{H}_{\{P_n\}}. \quad (2)$$

where the different $\mathcal{H}_{\{P_k\}}$ terms are expressed in the following form:

$$\mathcal{H}_{\{P_k\}}=\sum_{\text{all indexes}} t^{\Omega(K,n\Gamma)\Gamma_v\Gamma'_v}_{\{s\}\{s'\}}\beta\left[{}^{\varepsilon}V^{\Omega_v(\Gamma_v\Gamma'_v)\Gamma}_{\{s\}\{s'\}}\otimes R^{\Omega(K,n\Gamma)}\right]^{(A_1)}. \quad (3)$$

In this equation, the $t^{\Omega(K,n\Gamma)v\Gamma'v}_{\{s\}\{s'\}}$ are the parameters to be determined, while ${}^{\varepsilon}V^{\Omega_v(\Gamma_v\Gamma'_v)\Gamma}_{\{s\}\{s'\}}$ and $\mathrm{R}^{\Omega(K,n\Gamma)}$ are vibrational and rotational operators, respectively.

For each term, Ω_v and Ω represent the degree in elementary vibrational operators (creation a^+ and annihilation a operators), and rotational operators (components J_x, J_y and J_z of the angular momentum), respectively. β is a factor that allows the scalar terms (terms with $\Gamma = A_1$, the totally symmetric irreducible representation of T_d) to match the "usual" contributions like $B_0 J^2$, *etc.* The order of each individual term is defined as $\Omega + \Omega_v - 2$. We deal with the effective Hamiltonians which are obtained, for a given polyad P_k, by the projection of H in the P_n Hilbert subspace:

$$\begin{aligned} H^{<P_n>} &= P^{<P_n>} \mathcal{H} P^{<P_n>} \\ &= H^{<P_n>}_{\{\mathrm{GS}\}} + H^{<P_n>}_{\{P_1\}} + \ldots + H^{<P_n>}_{\{P_k\}} + \ldots + H^{<P_n>}_{\{P_{n-1}\}} + H^{<P_n>}_{\{P_n\}}. \end{aligned} \tag{4}$$

This effective Hamiltonian contains all the operators, and thus all the parameters, of the lower polyads. Parameters of upper polyads are (presumably) small corrections to those of the lower ones since in our model they are in fact differences between lower and upper state values; this is what we call "vibrational extrapolation". It enables global fits of data for a series of consecutive polyads, ensures a global consistency and, usually, a better convergence of molecular parameters. Just in order to give a simple illustrative example, if we consider a polyad P_1 containing a fundamental band, then the effective Hamiltonian $H^{<P_1>} = H^{<P_1>}_{\{\mathrm{GS}\}} + H^{<P_1>}_{\{P_1\}}$ contains in $H^{<P_1>}_{\{\mathrm{GS}\}}$ the ground state rotational constant B_0 and in $H^{<P_1>}_{\{P_1\}}$ the difference $\Delta B = B_1 - B_0$, that is the difference between the upper (say, B_1) and lower (B_0) state rotational constants, and not B_1 itself. We usually have $\Delta B \ll B_0, B_1$.

3.2. Polyad scheme definition

Generally speaking, the polyad number n can be defined as

$$n = i_1 v_1 + i_2 v_2 + i_3 v_3 + i_4 v_4, \tag{5}$$

where v_1, v_2, v_3 and v_4 are vibrational quantum numbers for the four normal modes of the molecule, while i_1, i_2, i_3 and i_4 are integer numbers chosen to group vibrational levels (v_1, v_2, v_3, v_4) into polyads, according to their wavenumbers.

In particular, when some vibrational numbers display simple approximate ratios, a clear polyad structure may appear. For instance, the well-known polyad structure of methane [33] comes from the fact that $\widetilde{\nu}_1 \simeq \widetilde{\nu}_3 \simeq 2\widetilde{\nu}_2 \simeq 2\widetilde{\nu}_4$, leading to large absorbing bands which are regularly spaced, each 1500 cm^{-1}. In the case of CF_4, however, no such global approximate relation exists. In Ref. [23], it was just noticed that $\widetilde{\nu}_3 \simeq 2\widetilde{\nu}_4$, implying to place the $v_3 = 1$ and $v_4 = 1$ vibrational levels in the same polyad. Thus, contrary to what is done for CH_4, it appears difficult to include all modes in a single polyad scheme at this stage. We thus decided here to build two separate polyad schemes:

- A "ν_2" polyad scheme implying the ν_2 bending mode, its overtones and combinations and related bands linked to it through combinations (in fact, almost "all" the lowest CF_4 bands not linked with the ν_1 mode). In this case, we choose:

$$n_{\nu_2} = 2v_2 + 6v_3 + 3v_4. \tag{6}$$

- A "ν_1" polyad scheme implying the ν_1 stretching mode influence into several bands. In this case, we choose:

$$n_{\nu_1} = 3v_1 + 4v_3 + 2v_4. \tag{7}$$

In both cases, there is no polyad number 1 (this one has no corresponding vibrational level). As we will see later, these two schemes lead to two separate global effective Hamiltonian fits. Tables 3 and 4 list essential details on the polyads including the number of operators for the "ν_2" and "ν_1"schemes, respectively. All vibrational quantum numbers are limited to the values 0, 1 and 2. Except for the (non-existing) polyad number 1, all effective Hamiltonian contributions have been expanded up to the 8th order. In the final analysis, however (see Section 4), only a small subset of all the resulting parameters could be actually determined from the fit, as indicated in the last column of both tables.

Figure 2 shows the transitions included in the two fits, corresponding to the two polyad schemes. These fits are described in Section 4 below.

Polyad	Vibrational levels	Order	Nb. parameters	Nb. fitted
0	(0,0,0,0)	8	15	10
1	—	0	0	0
2	$(0,1,0,0)$	8	26	12
3	$(0,0,0,1)$	8	48	17
4	$(0,2,0,0)$	8	29	6
5	$(0,1,0,1)$	8	84	9
6	$(0,0,1,0),(0,0,0,2)$	8	224	51
7	$(0,2,0,1)$	8	78	0
8	$(0,1,1,0),(0,1,0,2)$	8	383	92
	Total		887	197

Table 3: Effective Hamiltonian for the "ν_2" scheme, with the number of parameters in the model. Vibrational levels are denoted using vibrational quantum numbers in the form (v_1, v_2, v_3, v_3). The last column shows the number of parameters that could be fitted (see Section 4.1).

3.3. Line intensity calculations

In order to calculate transition intensities, the effective dipole moment transition operator is also determined in a similar way (see Ref. [32] for more detail). This operator is expanded to the lowest possible degree. In the case of the $\nu_3/2\nu_4$ dyad, we use the same dipole moment expansion as in our previous paper [23]. Dipole moment derivative values and line intensities in this strongly absorbing ν_3 region are discussed in Section 5.

3.4. Basis sets

The calculation of the effective Hamiltonian and effective dipole moment matrix elements are performed in the coupled rovibrational basis

$$\left|\left[\Psi_v^{(C_v)} \otimes \Psi_r^{(J,nC_r)}\right]^{(C)}\right\rangle, \tag{8}$$

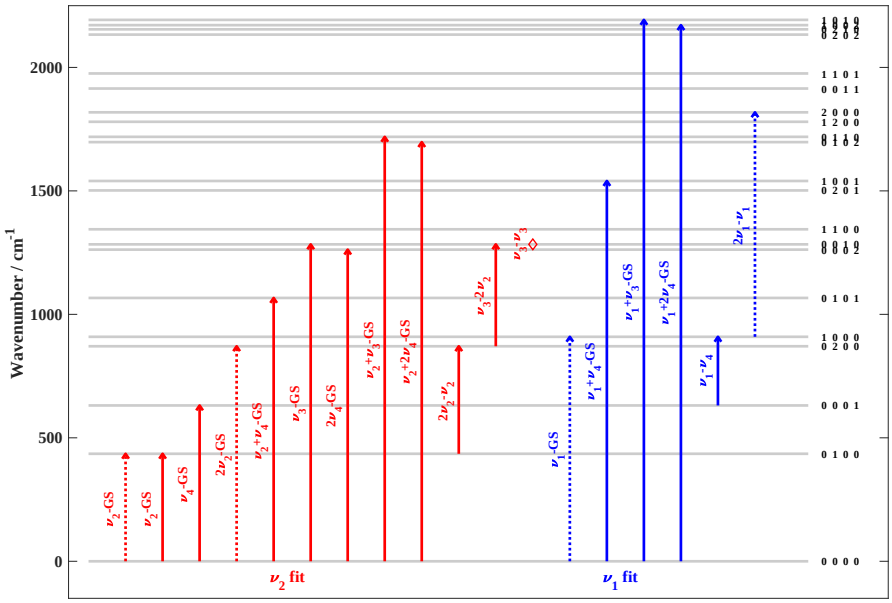

Figure 2: Vibrational transitions and levels used in the two fits. Dashed lines correspond to Raman transitions. The ν_2 fundamental band is observed both in infrared absorption and Raman scattering (see text).

Polyad	Vibrational levels	Order	Nb. parameters	Nb. fitted
0	(0,0,0,0)	8	15	0†
1	—	0	0	0
2	$(0,0,0,1)$	8	48	0†
3	$(1,0,0,0)$	8	11	7
4	$(0,0,1,0), (0,0,0,2)$	8	224	0†
5	$(1,0,0,0)$	8	27	24
6	$(2,0,0,0), (0,0,1,1)$	8	214	3‡
7	$(1,0,1,0), (1,0,0,2)$	8	109	73
	Total		648	107

† Parameters fixed to the values from the "ν_2" fit, see Table 3.

‡ Only $v_1 = 2$ parameters are fitted.

Table 4: Effective Hamiltonian for the "ν_1" scheme, with the number of parameters in the model. Vibrational levels are denoted using vibrational quantum numbers in the form (v_1, v_2, v_3, v_3). The last column shows the number of parameters that could be fitted (see Section 4.2).

where $\Psi_r^{(J,nC_r)}$ is a rotational wavefunction with angular momentum J, rotational symmetry species C_r and multiplicity index n; $\Psi_v^{(C_v)}$ is a coupled vibrational basis set; C is the overall symmetry species ($C = C_v \otimes C_r$). $\Psi_v^{(C_v)}$ contains the relevant functions for the 4 normal modes of vibration,

$$\left|\Psi_v^{(C_v)}\right\rangle = \left|((\Psi_{v_1}^{(A_1)} \otimes \Psi_{v_2}^{(l_2,C_2)} \otimes \Psi_{v_3}^{(l_3,n_3C_3)})^{(C_{23})} \otimes \Psi_{v_4}^{(l_4,n_4C_4)})_{\sigma_v}^{(C_v)}\right\rangle \quad (9)$$

For each normal mode number $i = 1$ to 4, we use a symmetrized harmonic oscillator basis set denoted

$$\left|\psi_{v_i}^{(l_i,n_iC_i)}{}_{\sigma_i}\right\rangle = |v_i, l_i, n_iC_i, \sigma_i\rangle\,, \quad (10)$$

where

$$l_1 = 0, \quad (11)$$

$$l_i = v_i, v_i - 2, v_i - 4, \ldots, 0 \text{ or } 1 \ (i = 2, 3 \text{ or } 4), \quad (12)$$

are the usual vibrational angular momentum quantum numbers for degenerate vibrations. C_i is a T_d irreducible representation (irrep) and n_i a multiplicity index used when C_i appears more than once for a given (v_i, l_i) set. We always have $n_1 = 0$, $n_2 = 0$ and necessarily $C_1 = A_1$. In Equation (9), we have:

$$C_{23} = C_2 \otimes C_3 \qquad \text{and} \qquad C = C_{23} \otimes C_4, \tag{13}$$

C_v being the overall vibrational symmetry. All C symbols here represent T_d irreps.

4. Global fits of line positions

As already mentioned, the philosophy of this work is to gather many CF_4 high-resolution spectroscopic data (see Table 2) to use them in global fits of line positions. Just as explained in Section 3.2, it appears difficult to include all CF_4 vibrational levels in a single polyad scheme. As a matter of fact, contrary to methane (CH_4) which has a well-defined polyad structure [33, 34, 35], CF_4 has fundamental vibrational wavenumber with a more random distribution; we can just notice, as in our previous work [23], that $\widetilde{\nu}_3$ is close to $2\widetilde{\nu}_4$ leading to a Fermi interaction between the corresponding bands that must be treated as a dyad. This interaction propagates to all combination bands built on $\nu_3/2\nu_4$, for instance when adding ν_1 or ν_2 quanta.

Thus, it appeared wise and more practical to perform assignments and effective Hamiltonian fit following two partial polyad schemes. These two schemes are described in Section 3.2 and the two sections below describe the assignment and fit process in each case.

It should be noticed that during the fits the different sets of data were used with the same weights due to compatible quality of the experimental spectra (see Section 2).

4.1. Global fit based on the ν_2 mode

The fundamental band of the ν_2 mode of tetrahedral XY_4 molecules is, at first approximation, only active in Raman scattering. A few years ago, we could

analyze this fundamental band thanks to high-resolution stimulated Raman spectroscopy [24]. This excellent technique can provide essential data for such non-infrared active modes [36, 37, 38, 39, 24] but has also some drawbacks: its spectral resolution (around 0.003 cm^{-1}) and sensitivity are significantly lower that what can be achieved using infrared absorption spectroscopy. In some cases, however, ν_2 can gain intensity from rovibrational coupling with another vibrational mode. This is the case for methane, for instance, whose $\widetilde{\nu}_2$ and $\widetilde{\nu}_4$ wavenumbers are quite close to each other [40], so that the two corresponding fundamentals form a bending dyad. Although these two modes are more separated for CF_4, a weak ν_2 fundamental band is observable in the 400–470 cm^{-1} region when a long optical path length is used [29]. In other words, the weakness of this interaction does not necessitate to consider a $v_2 = v_4 = 1$ polyad, but its influence on the ν_2 induced dipole moment is sufficient to let this fundamental band appear in infrared absorption. In the present work, we used such a spectrum (see Section 2 and Table 2), along with the existing Raman data from Ref. [24].

We then included new data concerning the $\nu_2 + \nu_4$ combination band. Analyzing this one implies to know the $v_4 = 1$ level itself, so the previous data on the ν_4 fundamental [23] were necessary. As this one was already a part of a global study including the $\nu_3/2\nu_4$ dyad (see above), we also included data corresponding to this region, coming both from Ref. [23] and from newly recorded spectra (Table 2). Some recently recorded THz lines of the $\nu_3 - \nu_3$ hot band are also used [28]. Finally, a new $\nu_2 + (\nu_3/2\nu_2)$ spectrum was also considered, leading to a global analysis and fit of all rovibrational bands that do not imply the ν_1 mode in the 0 to 1750 cm^{-1} region. We also noticed that the new spectra allowed to assign some hot band lines for $2\nu_2 - \nu_2$ and $\nu_3 - 2\nu_2$ in the ν_2 infrared spectrum, which completed the dataset. As explained in Section 3.2 and Table 3, this is referred as the "ν_2" scheme and fit.

We can notice that this study allowed to refine the GS parameters. It was also necessary to correct some ν_2, $2\nu_2$ and $\nu_3/2\nu_4$ assignments from our previous papers [23, 24]. ν_4 and $\nu_3/2\nu_4$ are now assigned up to slightly higher J values.

The analysis was performed thanks to the STDS [41] package of the XTDS software [42] which allows to calculate and fit XY_4 spherical-top spectra. All assignments have been performed with help of the SPVIEW complementary software [42]. A total of 17,626 lines could be assigned (see Table 5) to determine 197 effective Hamiltonian parameters (see Table 3). The overall root mean square deviation is 1.116×10^{-3} cm^{-1}. For each of the new spectra, initial simulations were performed using the existing effective Hamiltonian parameters from the previous studies which yielded preliminary assignments. Then the new parameters were determined and the assignments refined. Some corrections were also made to the assignments form the previous works. The process was iterated till no more assignment appeared possible.

Table 5 summarizes the fit statistics and Figure 3 displays the fit residuals for line positions. Table A.6 in the Appendix gives the effective Hamiltonian parameter values. Concerning the ν_2 fundamental band itself, it should be noticed that we now have 3.2 times more lines, for J up to 82, instead of 45, compared to Ref. [24].

We give four examples of comparisons between experiment and simulation in spectral regions in infrared absorption, which are analyzed and modeled here for the first time. Figure 4 presents the interaction-induced ν_2 region for which we could analyse and simulate two hot bands, namely $2\nu_2 - \nu_2$ and $\nu_3 - 2\nu_2$. Figure 5 represents the same region at a high pressure, the experimental data being those used for Figure 1 of Ref. [29]. For these first two examples, the vertical scale of the simulations has been adjusted manually to match with the experimental spectra. No attempts to determine absolute intensities has been performed in this case, contrary to what is discussed in Section 5 below for the strongly absorbing ν_3 region. Figure 6 displays the $\nu_2 + \nu_4$ region. Figure 7 shows some details concerning the quite complex $\nu_2 + (\nu_3/2\nu_4)$ region. This one has 8 vibrational sublevels. We illustrate this on Figure 8, which displays the rovibrational sublevels, as a function of the rotational quantum number J.

Transitions	Number of data	$J_{\max}$	σ	d_{RMS} / 10^{-3} cm^{-1}
		"ν_2" fit		
ν_2	4686	82	0.9984	1.027
ν_4	2254	72	1.276	1.276
$2\nu_2$	823	42	0.7757	0.7757
$\nu_2+\nu_4$	877	39	1.188	1.188
$\nu_3/2\nu_4$	2930	53	0.9847	1.161
$\nu_2+(\nu_3/2\nu_4)$	4763	49	1.167	1.167
$2\nu_2-\nu_2$	803	68	0.7758	0.7758
$\nu_3-2\nu_2$	222	37	1.189	1.189
$\nu_3-\nu_3$	268	37	0.9173	33.64 MHz
Total	17626	82	1.076	1.116
		"ν_1" fit		
ν_1	2368	83	0.3498	1.049
$\nu_1+\nu_4$	669	47	0.4689	0.8687
$\nu_1-\nu_4$	2524	64	1.043	1.043
$\nu_1+(\nu_3/2\nu_4)$	3094	74	1.608	1.825
$2\nu_1-\nu_1$	229	73	3.068	0.6968
Total	8884	83	1.225	1.354

Table 5: Fit statistics for the two polyad schemes. σ is the dimensionless standard deviation and d_{RMS} the root mean square deviation in 10^{-3} cm^{-1}, except for THz $\nu_3-\nu_3$ lines for which it is given in MHz.

More precisely, this Figure shows the reduced energy levels, defined by:

$$\begin{aligned}\widetilde{\nu}_{\mathrm{red}} &= \widetilde{\nu} - \sum_{\Omega} t^{\Omega(0,0A_1)A_1A_1}_{\{\mathrm{GS}\}\{\mathrm{GS}\}}(J(J+1))^{\Omega/2} \\ &= \widetilde{\nu} - B_0J(J+1) + D_0J^2(J+1)^2 - \ldots, \end{aligned} \tag{14}$$

i.e. we subtract the dominant scalar polynomial terms in order to enhance levels splittings due to molecular symmetry. We give both the calculated and observed reduced energy levels. Observed levels are simply levels reached by assigned transitions which are included in the fit. This gives a good idea of the sampling of the energy spectrum.

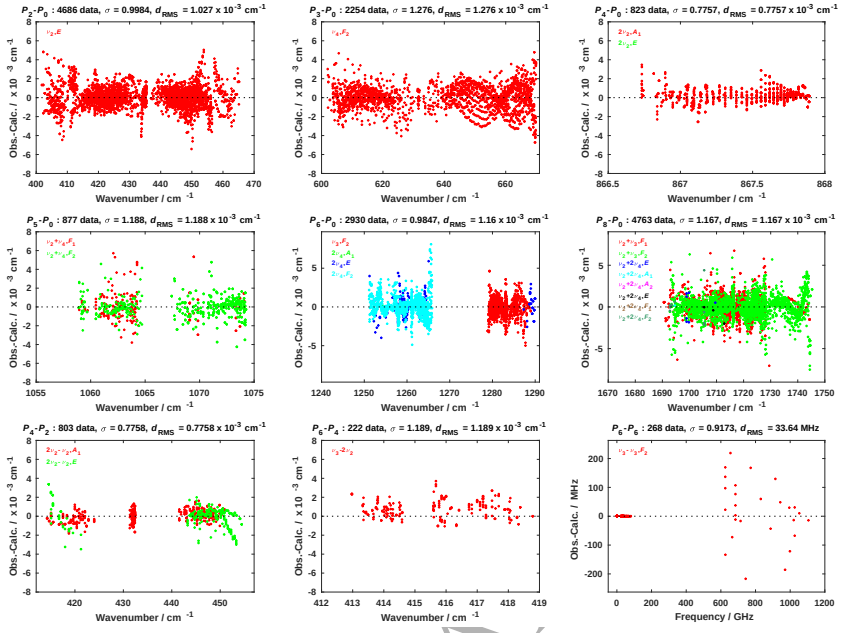

Figure 3: Fit residuals for line positions, in the case of the "ν_2" fit. In each spectral region, the colors correspond to the different vibrational sublevels.

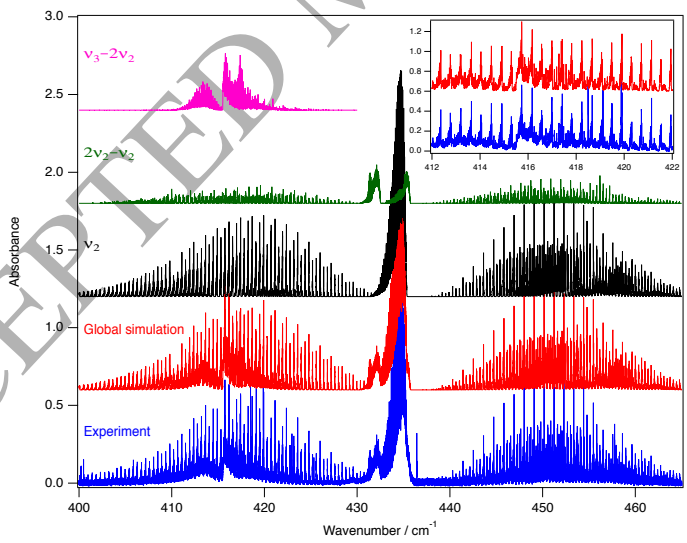

Figure 4: Measured ν_2 spectral region in infrared absorption at 296 K and 18 Torr, compared to the simulation with two hot bands. The insert details a part of the P branch, around the $\nu_3 - 2\nu_2$ region.

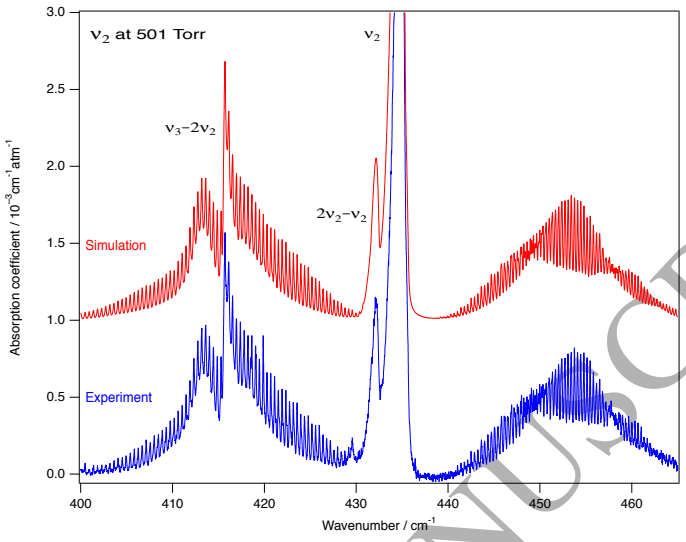

Figure 5: Measured ν_2 spectral region at 296 K and high pressure (501 Torr, see Table 2 and Ref. [29]), compared to the simulation with two hot bands.

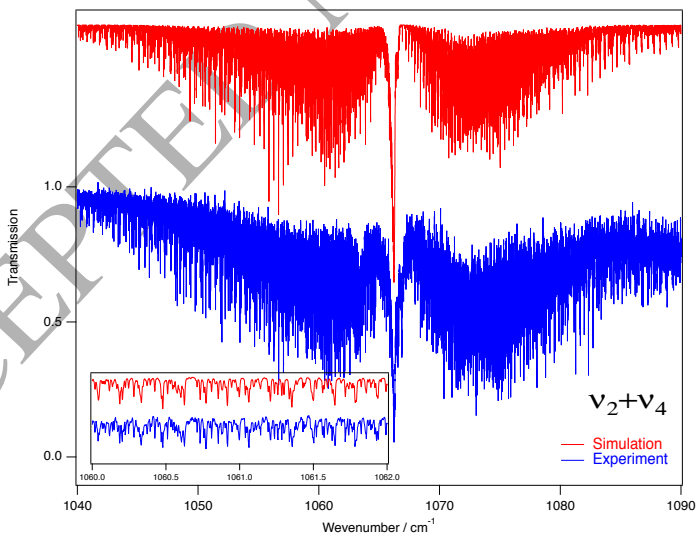

Figure 6: Measured $\nu_2 + \nu_4$ difference band at 296 K and 11.25 Torr, compared to the simulation. The insert details a part of the P branch.

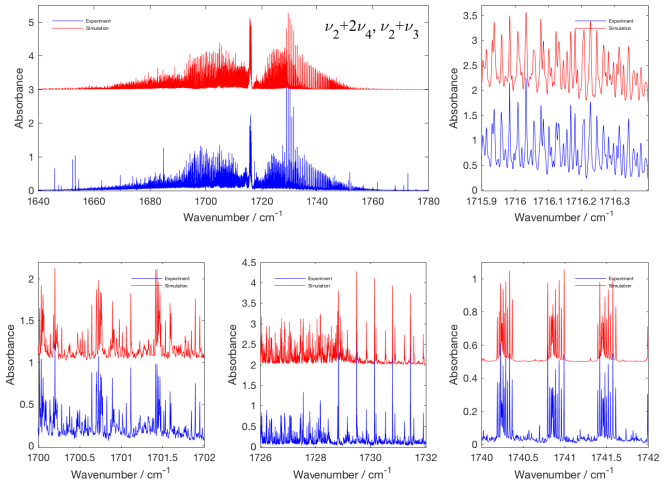

Figure 7: Measured spectrum in the $\nu_2 + (\nu_3/2\nu_4)$ region (295 K, 5 Torr), compared to the simulation, with detailed view of some parts. Strong lines on the wings are water vapor lines.

4.2. Global fit based on the ν_1 mode

Just as for ν_2, the totally symmetric ν_1 stretching mode is, in first approximation, only Raman-active. Contrary to the CH_4 case [43] and to what happens with ν_2 (see previous Section), rovibrational interaction-induced ν_1 lines are too weak to be observed in infrared absorption. Thus, up to now, high-resolution stimulated Raman spectroscopy was the only data source for this mode [24]. The Raman spectrum of ν_1 only displays a narrow Q branch for the ν_1 fundamental band, which strongly limits the number of assignable lines.

Recently, in the case of the SF_6 molecule, we have shown another way to access such modes using the difference bands [44]. As a matter of fact, the far infrared region of CF_4 near 280 cm^{-1} displays a very nice $\nu_1 - \nu_4$ band with a well-defined PQR branches structure. As described in Section 2, the

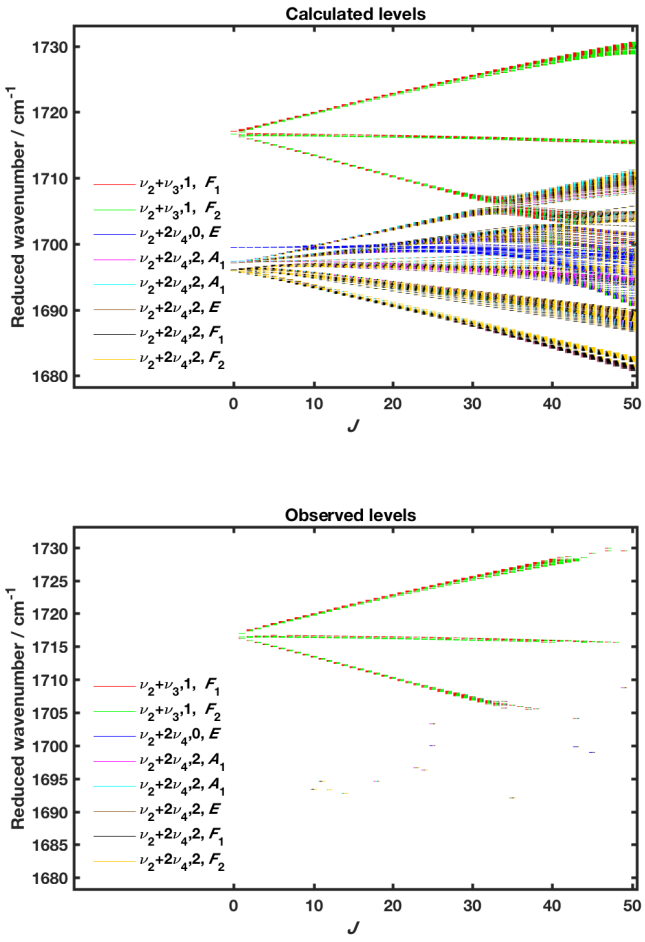

Figure 8: Observed and calculated reduced rovibrational energy levels for the $\nu_2 + (\nu_3/2\nu_4)$ region, compared to the simulation. "Observed" levels correspond to those reached by assigned transitions. The colors represent the mixings between the different sublevels.

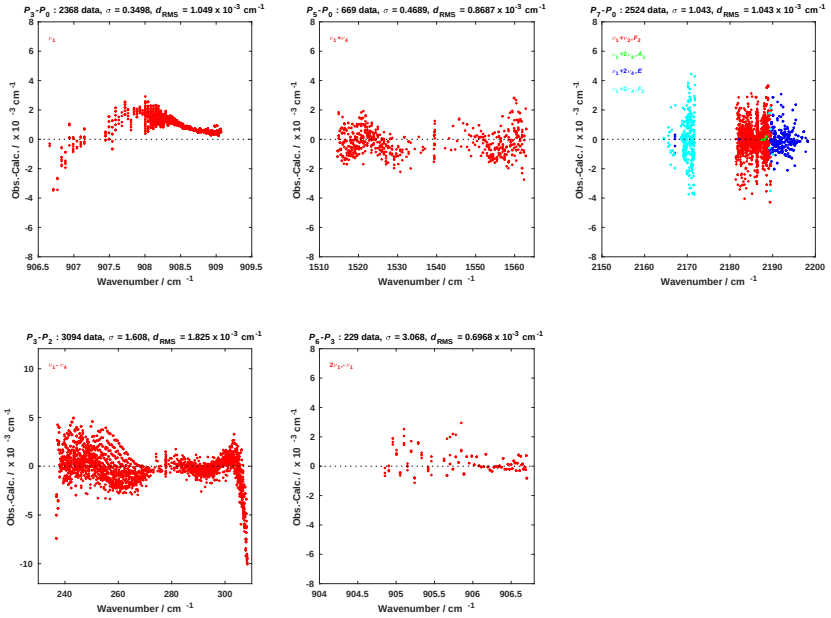

Figure 9: Fit residuals for line positions, in the case of the "ν_1" fit. In each spectral region, the colors correspond to the different vibrational sublevels.

synchrotron radiation was of a great help to obtain spectra with an excellent signal-to-noise ratio in this low wavenumber region.

It made it possible to perform a new global analysis including vibrational levels implying the ν_1 mode. This includes ν_1 and $2\nu_1 - \nu_1$ Raman lines, and new spectra for $\nu_1 - \nu_4$, $\nu_1 + \nu_4$ and $\nu_1 + (\nu_3/2\nu_4)$. As explained in Section 3.2 and Table 4, this is referred as the "ν_1" scheme and fit. Parameters for the ground state, $v_4 = 1$, $v_4 = 2$ and $v_3 = 1$ levels were fixed to the values obtained in the "ν_2" fit. The reason is that, in this second case, we have less data and less parameters to fit. The line assignment and fit and simulation procedures using the XTDS and SPVIEW softwares [42] were totally similar to what we did for the "ν_2" fit (see previous Section).

Table 5 summarizes the fit statistics and Figure 9 displays the fit residuals for line positions. Table B.7 in the Appendix lists the effective Hamiltonian parameter values.

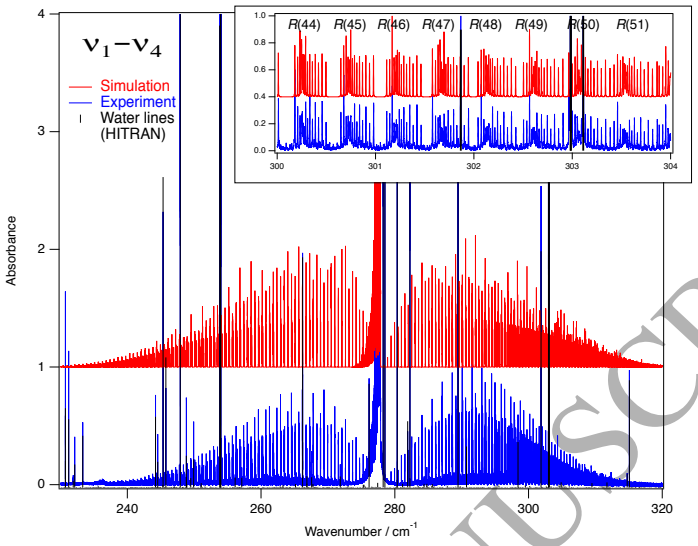

Figure 10: Measured $\nu_1 - \nu_4$ difference band at 296 K and 18 Torr, compared to the simulation. Strong lines peaks are water vapor lines. The insert details a part of the R branch.

Figure 10 displays the $\nu_1 - \nu_4$ region, compared to the simulation. The insert nicely illustrates the well-defined fine structure in the P branch. Figure 11 shows the $\nu_1 + (\nu_3/2\nu_4)$ region. This one has 4 vibrational sublevels. Figure 12 displays the calculated and observed reduced energy levels, as defined by Equation 14.

4.3. Discussion

In Ref. [24], we calculated the equilibrium bond length r_e of CF_4. This calculation is possible if one knows the value of the rotational constant B_0 in the ground state and rotational constant differences in all the vibrational

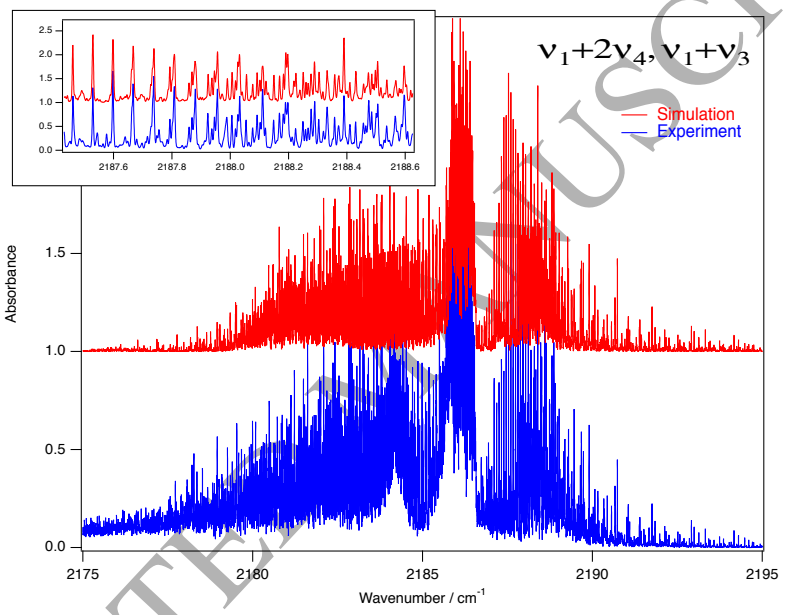

Figure 11: Measured spectrum of the $\nu_1 + (\nu_3/2\nu_4)$ region at 295 K and 0.5 Torr, compared to the simulation. The insert details a part of the R branch. The strong Q branch near 2183 cm^{-1} is the $\nu_1 + \nu_3 + \nu_2 - \nu_2$ hot band, which is not simulated here.

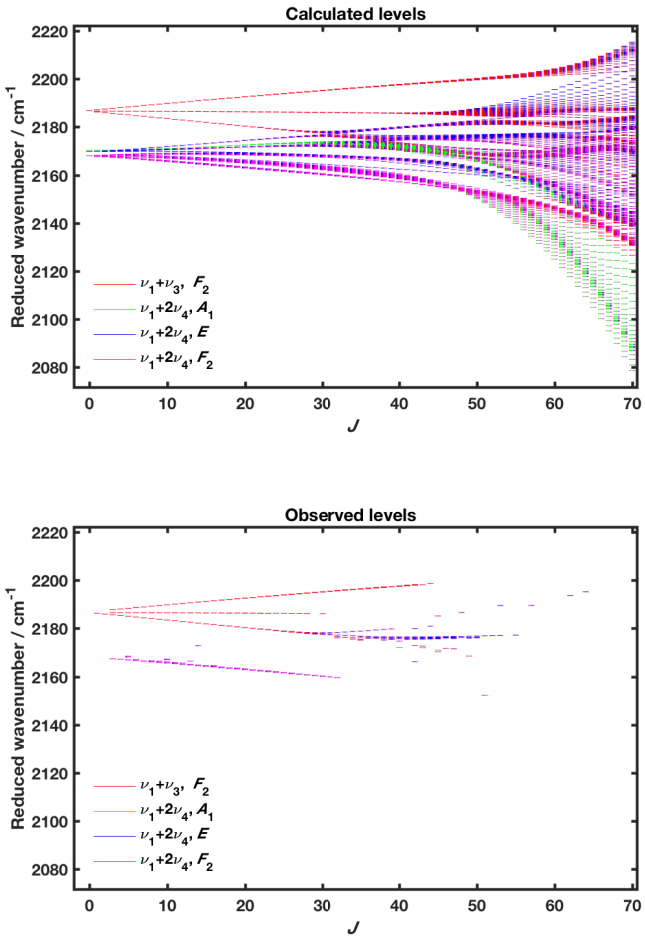

Figure 12: Observed and calculated reduced rovibrational energy levels for the $\nu_1 + (\nu_3/2\nu_4)$ region, compared to the simulation. "Observed" levels correspond to those reached by assigned transitions. The colors represent the mixings between the different sublevels.

fundamental levels, say $\Delta B_i = B_i - B_0$ ($i = 1, \ldots, 4$), where B_i is the rotational constant in an excited state with $v_i = 1$. The formula giving B_e is [36]:

$$B_e = B_0 - \frac{1}{2}\sum_{i=1}^{4} d_i \Delta B_i, \tag{15}$$

where d_i is the normal mode degeneracy ($d_1 = 1$, $d_2 = 2$, $d_3 = d_4 = 3$). The equilibrium bond length is:

$$r_e = \sqrt{\frac{3h}{64\pi^2 c m_{\mathrm{F}} B_e}}, \tag{16}$$

h being Planck's constant and m_{F} the fluorine atom's mass. The fitted parameters $\Delta B_i = t^{2(0,0A_1)\Gamma_v\Gamma_v}_{\{i\}\{i\}}$ result from the two previous global fits. Using their values and standard deviation taken from Tables A.6 and B.7, we get:

$$B_e = 0.1924649(61)\ \mathrm{cm}^{-1}, \tag{17}$$

and thus:

$$r_e = 1.314860(21)\ \text{Å}. \tag{18}$$

This value is slightly smaller than in Ref. [24], but more precise.

5. Line intensities

Using the present results about the $v_2 = v_3 = 1/v_4 = 2$ level ($\nu_2 + (\nu_3/2\nu_4)$ dyad region) and of $v_1 = v_3 = 1/v_4 = 2$ level ($\nu_1 + (\nu_3/2\nu_4)$ dyad region), it becomes possible to calculate the $\nu_3 + \nu_2 - \nu_2$, $2\nu_4 + \nu_2 - \nu_2$, $\nu_3 + \nu_1 - \nu_1$ and $2\nu_3 + \nu_1 - \nu_1$ hot bands, in the $\nu_3/2\nu_4$ region. In order to calculate absolute line intensities, we can use the ν_3 and $2\nu_4$ dipole moment derivative parameters from Ref. [45] (see also Section 5 of Ref. [23] for more explanations). These two values are sufficient and common to both cold and hot bands, when limiting the dipole moment operator expansion to degree 1. No further dipole moment refinement is possible, since no individual line intensity measurement is available, due to the spectroscopic congestion for this molecules, for which almost all observed lines result from the overlap of several transitions.

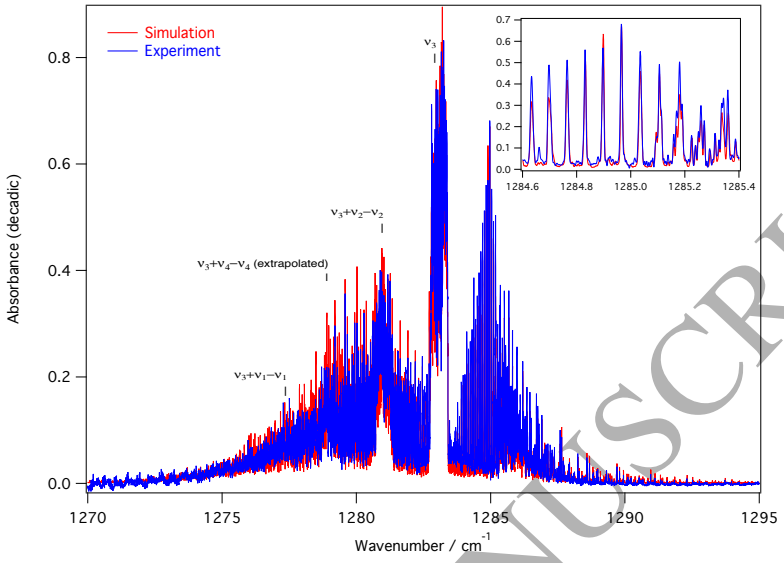

Figure 13: Experimental spectrum in the ν_3 region (296 K, 17 Torr), including hot bands, compared to the simulation. The insert details a part of the R branch. Most of the absorption intensity is well reproduced by the model.

It is even possible to extrapolate the $\nu_3 + \nu_4 - \nu_4$ and $3\nu_4 - \nu_4$ hot bands, although the corresponding vibrational levels could not be assigned in the current work. These would be a part of the polyad number 9 in the "ν_2" polyad scheme, whose effective Hamiltonian can expanded up to order two only, leading to purely vibrational parameters only. We just set up the four parameters of the $v_3 = v_4 = 1$ vibrational level (corresponding to the anharmonicity coefficient of its four sublevels) to a constant value of -4.7 cm^{-1}, corresponding to a correct positioning of the $\nu_3 + \nu_4 - \nu_4$ Q branch (see Figures 13 and 14 below).

The resulting simulation at high resolution is shown on Figure 13, compared to the corresponding spectrum recorded in the present work. Figure 14 shows a low-resolution simulation, compared to a band profile from the PNNL database [46].

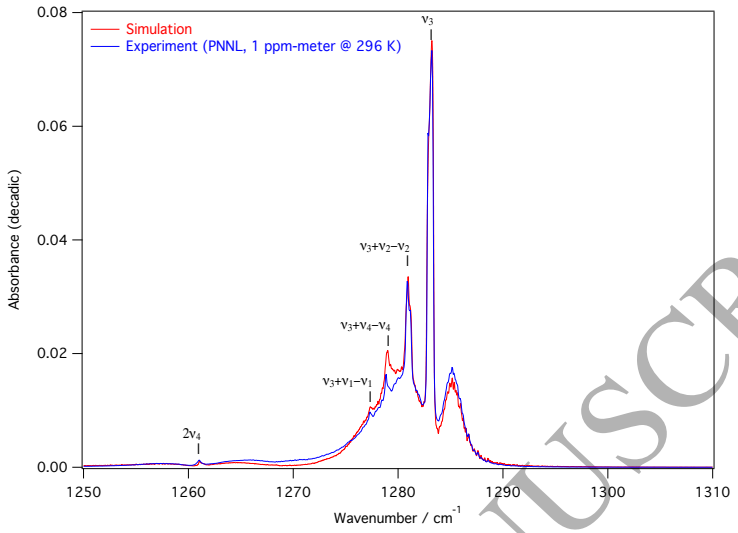

Figure 14: PNNL (see text and Ref. [46]) spectrum of the ν_3 region, including hot bands, at low resolution, compared to the simulation.

It appears clearly that we can now simulate a significant part (almost 92 %, see Figure 1) of the ν_3 region absorption intensity at room temperature, compared to the sole ν_3 fundamental simulation (which represents only 65.8 % of the intensity).

6. HITRAN and TFMeCaSDa updates

Although the present work was not fully ready on time for the recent HITRAN 2016 [18] and GEISA 2015 [20] updates, a new partial calculated line list including ν_3 and $\nu_3 + \nu_2 - \nu_2$ only could be used for the HITRAN 2016 update itself. Then, the complete CF_4 line list in the ν_3 region, including hot bands based on ν_1, ν_2 and ν_4 (see previous Section) has now been accepted by these databases for an intermediate online update.

Moreover, we have previously setup a database named TFMeCaSDa (*Tetra-Fluoro-Methane Calculated Spectroscopic Database*) of the calculated CF_4 spectroscopic lines in the framework of the *Virtual Atomic and Molecular Data Cen-*

tre (VAMDC) [47, 48, 49]. This one has also been updated using the present data. It is accessible through the VAMDC portal (http://portal.vamdc.org).

7. Conclusion

The two global fits presented in this study constitute the most extensive study of CF_4 rovibrational levels to date. This enables a significant update of the public spectroscopic databases concerning this molecule. Our results should allow a much better modeling of the atmospheric absorption and improved concentration retrievals from satellite, balloon-borne and ground-based data.

The next step will be to include even more bands in the analysis, possibly in a unique global polyad scheme, if possible. In particular, the $\nu_3 + \nu_4$ band should be assigned and analyzed in detail. The knowledge of this one would lead to the calculation of the $\nu_3 + \nu_4 - \nu_4$ hot band, which is the second one in terms of absorption intensity, representing 9.2 % of it in the ν_3 region at room temperature (here, we could just extrapolate this band). This kind of rovibrational system is quite challenging to analyze, since the $v_3 = v_4 = 1$ vibrational level has four sublevels whose exact position is still unknown. Presumably, *ab initio* calculations would be of help to get initial values for these anharmonicity coefficients. Moreover, this band should interact with $3\nu_4$.

Another important challenge would be to accurately measure the line intensities and to determine the experimental dipole moment parameters, instead of using previously calculated values. This is not an easy task, for such a heavy molecule with a very congested spectrum consisting mostly of many overlapping lines.

8. Acknowledgements

MC wishes to thank OSU THETA ("*Observatoire des Sciences de l'Univers Terre Homme Environnement Temps Astronomie de Franche-Comté/Bourgogne*") for financial support during his stay in Reims to perform experiments at the GSMA laboratory.

References

[1] A. R. Ravishankara, S. Solomon, A. A. Turnipseed, R. F. Warren, Atmospheric lifetimes of long-lived halogenated species, Science 259 (1993) 194–199.

[2] R. A. Morris, T. M. Miller, A. A. Viggiano, J. F. Paulson, S. Solomon, G. Reid, Effects of electron and ion reactions on atmospheric lifetimes of fully fluorinated compounds, J. Geophys. Res. D 100 (1995) 1287–1294.

[3] J. Harnisch, D. de Jager, J. Gale, O. Stobbe, Halogenated compounds and climate change: Future emission levels and reduction costs, Environ. Sci. & Pollut. Res. 9 (6) (2002) 369–374.

[4] J. Harnisch, N. Höhne, Comparison of emissions estimates derived from atmospheric measurements with national estimates of HFCs, PFCs and SF_6, Environ. Sci. & Pollut. Res. 9 (5) (2002) 315–320.

[5] V. Boudon, J.-P. Champion, T. Gabard, G. Pierre, M. Loëte, C. Wenger, Spectroscopic tools for remote sensing of greenhouse gases CH_4, CF_4 and SF_6, Environ. Chem. Lett. 1 (2003) 86–91.

[6] C. P. Rinsland, E. Mathieu, R. Zander, R. Nassar, P. Bernath, C. Boone, L. S. Chiou, Long-term stratospheric carbon tetrafluoride (CF_4) increase inferred from 1985-2004 infrared space-based solar occultation measurements, Geophys Res. Lett. 33 (2006) L02808.

[7] J. Harnisch, R. Brochers, P. Fabian, H. Gäggeler, U. Schrotterer, Effect of natural tetrafluoromethane, Nature 384 (1996) 32.

[8] J. Harnisch, R. Borchers, P. Fabian, M. Maiss, Tropospheric trends for CF_4 and C_2F_6 since 1982 from SF_6 dated stratospheric air, Geophys. Res. Lett. 23 (1996) 1099–1102.

[9] D. A. Deeds, M. K. Vollmer, J. T. Kulongoski, B. R. Miller, J. Mühle, C. M. Harth, J. A. Izbicki, D. R. Hilton, R. F. Weiss, Evidence for crustal

degassing of CF_4 and SF_6 in Mojave Desert groundwaters, Geochim. et Cosmochim. Acta 72 (2008) 999–1013.

[10] M. A. K. Khalil, R. A. Rasmussen, J. A. Culbertson, J. M. Prins, E. P. Grimsrud, M. J. Shearer, Atmospheric perfluorocarbons, Environ. Sci. Technol. 37 (2003) 4358–4361.

[11] D. R. Worton, W. T. Sturges, L. K. Gohar, K. P. Shine, P. Martinerie, D. E. Oram, S. P. Humphrey, P. Begley, L. Gunn, J.-M. Barnola, J. Schwander, R. Mulvaney, Atmospheric trends and radiative forcings of CF_4 and C_2F_6 inferrer from firn air, Environ. Sci. Technol. 41 (2007) 2184–2189.

[12] J. Mühle, A. L. Ganesan, B. R. Miller, P. K. Salameh, C. M. Harth, B. R. Greally, M. Rigby, L. Porter, L. P. Steele, C. M. Trudinger, P. B. Krummel, S. O'Doherty, P. J. Fraser, P. G. Simmonds, R. G. Prinn, R. F. Weiss, Perfluorocarbons in the global atmosphere: tetrafluoromethane, hexafluoroethane, and octafluoropropane, Atmos. Chem. Phys. 10 (2010) 5145–5164.

[13] A. Goldman, D. G. Murcray, F. J. Murcray, G. R. Cook, J. W. V. Allen, F. S. Bonomo, R. D. Blatherwick, Identication of the ν_3 vibration-rotation band of CF_4 in balloon-borne infrared solar spectra, Geophys. Res. Lett. 6 (1979) 609–612.

[14] R. Zander, M. R. Gunson, C. B. Fanner, C. P. Rinsland, F. W. Irion, E. Mahieu, The 1985 chlorine and fluorine inventories in the stratosphere based on ATMOS observations at 30 north latitude, J. Atmos. Chem. 15 (1992) 171–186.

[15] R. Zander, S. Solomon, E. Mahieu, A. Goldman, C. Rinsland, M. R. Gunson, M. C. Abrams, A. Y. Chang, R. J. Salawitch, H. A. Michelsen, M. J. N. MJ, G. P. Stiller, Increase of stratospheric carbon tetrafluoride (CF_4) based on atmos observations from space, Geophys. Res. Lett. 23 (1996) 2353–2356.

[16] B. Sen, G. C. Toon, J.-F. Blavier, E. L. Fleming, C. H. Jackman, Balloon-borne observations of mid-latitude fluorine abundance, J. Geophys. Res. 101 (1996) 9045–9054.

[17] L. S. Rothman, I. E. Gordon, Y. Babikov, A. Barbe, D. C. Benner, P. E. Bernath, M. Birk, L. Bizzocchi, V. Boudon, L. R. Brown, A. Campargue, K. Chance, , E. A. Cohen, L. H. Coudert, V. M. Devi, S. Fally, B. J. Drouin, A. Fayt, J. M. Flaud, R. R. Gamache, J. J. Harrison, H. J.-M., C. Hill, J. T. Hodges, D. Jacquemart, A. Jolly, J. Lamouroux, R. Le Roy, G. Li, D. A. Long, L. O.M., M. C. J., S. T. Massie, S. Mikhailenko, H. Müller, O. V. Naumenko, A. V. Nikitin, J. Orphal, V. Perevalov, E. R. Perrin A. and-Polovtseva, C. Richard, S. M.A.H., E. Starikova, K. Sung, S. Tashkun, J. Tennyson, G. C. Toon, V. G. Tyuterev, G. Wagner, The HITRAN 2012 molecular spectroscopic database, J. Quant. Spectrosc. Radiat. Transfer 130 (2013) 4–50.

[18] I. E. Gordon, L. S. Rothman, R. V. C. Hill and, Y. Tan, P. F. Bernath, M. Birk, V. Boudon, A. Campargue, K. V. Chance, B. J. Drouin, J.-M. Flaud, R. R. Gamache, J. T. Hodges, D. Jacquemart, V. I. Perevalov, A. Perrin, K. P. Shine, M.-A. H. Smith, J. Tennyson, G. C. Toon, H. Tran, V. G. Tyuterev, A. Barbe, A. Csaszar, M. V. Devi, T. Furtenbacher, J. J. Harrison, A. Jolly, T. Johnson, T. Karman, I. Kleiner, A. A. Kyuberis, J. Loos, O. M. Lyulin, S. T. Massie, S. N. Mikhailenko, N. Moazzen-Ahmadi, H. S. P. M′uller, O. V. Naumenko, A. V. Nikitin, O. L. Polyan-sky, M. Rey, M. Rotger, S. Sharpe, K. Sung, E. Starikova, S. A. Tashkun, J. V. Auwera, G. Wagner, J. Wilzewski, P. Wcisło, S. Yu, E. J. Zak, The HITRAN2016 Molecular Spectroscopic Database, J. Quant. Spectrosc. Radiat. Transfer In press.

[19] N. Jacquinet-Husson, L. Crepeau, R. Armante, C. Boutammine, A. Chédin, N. A. Scott, C. Crevoisier, V. Capelle, C. Boone, N. Poulet-Crovisier, A. Barbe, A. Campargue, D. C. Benner, Y. Benilan, B. Bézard, V. Boudon, L. R. Brown, L. Coudert, A. Coustenis, V. Dana, V. M. Devi, S. Fally,

A. Fayt, J.-M. Flaud, A. Goldman, M. Herman, G. J. Harris, D. Jacquemart, A. Jolly, I. Kleiner, A. Kleinböhl, F. Kwabia-Tchana, N. Lavrentieva, N. Lacome, L.-H. Xu, O. Lyulin, J.-Y. Mandin, A. Maki, S. Mikhailenko, C. E. Miller, T. Mishina, N. Moazzen-Ahmadi, H. S. P. Müller, A. Nikitin, J. Orphal, V. Perevalov, A. Perrin, D. T. Petkie, A. Predoi-Cross, C. P. Rinsland, J. J. Remedios, M. Rotger, M. Smith, K. Sung, S. Tashkun, J. Tennyson, R. A. Toth, A.-C. Vandaele, J. V. Auwera, The 2009 edition of the GEISA spectroscopic database, J. Quant. Spectrosc. Radiat. Transfer 112 (2010) 2395–2445.

[20] N. Jacquinet-Husson, R. Armante, N. A. Scott, A. Chedin, L. Crepeau, C. Boutammine, A. Bouhdaoui, C. Crevoisier, V. Capelle, C. Boonne, N. Poulet-Crovisier, A. Barbe, D. C. Benner, V. Boudon, L. R. Brown, J. Buldyreva, A. Campargue, L. H. Coudert, V. M. Devi, M. J. Down, B. J. Drouin, A. Fayt, C. Fittschen, J. M. Flaud, R. R. Gamache, J. J. Harrison, C. Hill, O. Hodnebrog, S. M. Hu, D. Jacquemart, A. Jolly, E. Jimenez, N. N. Lavrentieva, A. W. Liu, L. Lodi, O. M. Lyulin, S. T. Massie, S. Mikhailenko, H. S. P. Mueller, O. V. Naumenko, A. Nikitin, C. J. Nielsen, J. Orphal, V. I. Perevalov, A. Perrin, E. Polovtseva, A. Predoi-Cross, M. Rotger, A. A. Ruth, S. S. Yu, K. Sung, S. A. Tashkun, J. Tennyson, V. I. G. Tyuterev, J. V. Auwera, B. A. Voronin, A. Makie, The 2015 edition of the GEISA spectroscopic database, J. Mol. Spectrosc. 327 (2016) 31–72.

[21] E. Mahieu, R. Zander, G. C. T. M. K. Vollmer, S. Reimann, J. Mühle, W. Bader, B. Bovy, B. Lejeune, C. Servais, P. Demoulin, G. Roland, P. F. Bernath, C. D. Boone, K. A. Walker, P. Duchatelet, Spectrometric monitoring of atmospheric carbon tetrafluoride (CF_4) above the Jungfraujoch station since 1989: evidence of continued increase but at a slowing rate, Atmos. Meas. Tech. 7 (2014) 333–344.

[22] D. Jackson, Statistical thermodynamic properties of hexafluoride molecules, Informal report LA-6025-MS, Los Alamos National Laboratory (1975).

[23] V. Boudon, J. Mitchell, A. Domanskaya, C. Maul, R. Georges, A. Benidar, W. G. Harter, High-resolution spectroscopy and analysis of the $\nu_3/2\nu_4$ dyad of CF_4, Mol. Phys. 109 (2011) 2273–2290.

[24] V. Boudon, D. Bermejo, R. Z. Martínez, High-resolution stimulated Raman spectroscopy and analysis of the ν_1, $2\nu_1 - \nu_1$, ν_2, $2\nu_2$, and $3\nu_2 - \nu_2$ bands of CF_4, J. Raman. Spectrosc. 44 (2013) 731–738.

[25] L. Régalia, Phd. thesis, University of Reims, France (1996).

[26] J.-J. Plateaux, A. Barbe, A. Delahaigue, Reims high-resolution Fourier-transform spectrometer – Data reduction for ozone, Spectrochim. Acta A 21 (1995) 1153–1159.

[27] V. Boudon, P. Asselin, P. Soulard, M. Goubet, T. Huet, R. Georges, O. Pirali, P. Roy., High-resolution spectroscopy and analysis of the $\nu_2 + \nu_3$ combination band of SF_6 in a supersonic jet expansion, Mol. Phys. 111 (2154–2162).

[28] V. Boudon, O. Pirali, M. Carlos, Pure rotation spectrum of CF_4 in the $v_3 = 1$ state using THz synchrotron radiation, To be published (2017).

[29] I. Grigoriev, A. V. Domanskaya, A. V. Podzorov, M. V. Tonkov, Intra- and intermolecular components of the ν_2 forbidden band of CF_4 in pure gas and in He, Ar, Xe and N_2 mixtures, Mol. Phys. 102 (2004) 1851–1857.

[30] V. Boudon, L. Manceron, F. K. Tchana, M. Loëte, L. Lago, P. Roy, Resolving the forbidden band of SF_6, Phys. Chem. Chem. Phys. 16 (2014) 1415–1423.

[31] V. Boudon, J.-P. Champion, T. Gabard, M. Loëte, F. Michelot, G. Pierre, M. Rotger, C. Wenger, M. Rey, Symmetry-adapted tensorial formalism to model rovibrational and rovibronic spectra of molecules pertaining to various point groups, J. Mol. Spectrosc. 228 (2004) 620–634.

[32] V. Boudon, J.-P. Champion, T. Gabard, M. Loëte, M. R. C. Wenger, Spherical top theory and molecular spectra, in: M. Quack, F. Merkt (Eds.), Handbook of High-Resolution Spectroscopy, Vol. 3, Wiley, Chichester, West Sussex, United Kingdom, 2011, pp. 1437–1460.

[33] V. Boudon, M. Rey, M. Loëte, The vibrational levels of methane obtained from analyses of high-resolution spectra, J. Quant. Spectrosc. Radiat. Transfer 98 (2006) 394–404.

[34] A. V. Nikitin, V. Boudon, C. Wenger, S. Albert, L. R. Brown, S. Bauerecker, M. Quack, High resolution spectroscopy and the first globalanalysis of the Tetradecad region of methane $^{12}CH_4$, Phys. Chem. Chem. Phys. 15 (2013) 10071–10093.

[35] B. Amyay, M. Louviot, O. Pirali, R. Georges, J. Vander Auwera, V. Boudon, Global analysis of the high temperature infrared emission spectrum of $^{12}CH_4$ in the dyad (ν_2/ν_4) region, The Journal of Chemical Physics 144 (2016) 024312–1–024312–15.

[36] V. Boudon, J. L. Doménech, D. Bermejo, H. Willner, High-resolution Raman spectroscopy of the ν_1 region and Raman-Raman double resonance spectroscopy of the $2\nu_1 - \nu_1$ band of $^{32}SF_6$ and $^{34}SF_6$. Determination of the equilibrium bond length of sulfur hexafluoride, submitted to J. Mol. Spectrosc. (2004).

[37] V. Boudon, D. Bermejo, First high-resolution Raman spectrum and analysis of the ν_5 bending fundamental of SF_6, J. Mol. Spectrosc. 213 (2002) 139–144.

[38] V. Boudon, J. L. Doménech, A. Ramos, D. Bermejo, H. Willner, High-resolution stimulated Raman spectroscopy and analysis of the ν_2, ν_5 and $2\nu_6$ bands of $^{34}SF_6$, Mol. Phys. 104 (16–17) (2006) 2653–2661.

[39] V. Boudon, D. Radhouani, M. Loëte, R. Z. Martínez, D. Bermejo, High-

resolution stimulated Raman spectroscopy and analysis of the ν_3 stretching band of GeD_4, J. Raman Spectrosc. 38 (2007) 559–562.

[40] J.-P. Champion, J.-C. Hilico, C. Wenger, L. R. Brown, Analysis of the ν_3/ν_4 dyad of $^{12}CH_4$ and $^{13}CH_4$, J. Mol. Spectrosc. 133 (1989) 256–272.

[41] C. Wenger, J.-P. Champion, Spherical top data system (STDS) software for the simulation of spherical top spectra, J. Quant. Spectrosc. Radiat. Transfer 59 (1998) 471–480.

[42] C. Wenger, V. Boudon, M. Rotger, M. Sanzharov, J.-P. Champion, XTDS and SPVIEW: Graphical tools for the analysis and simulation of high-resolution molecular spectra, J. Mol. Spectrosc. 251 (2008) 102–113.

[43] J.-C. Hilico, J.-P.Champion, S. Toumi, V. G. Tyuterev, A. S. Taskkun, New analysis of the pentad system of methane and prediction of the (pentad−pentad) spectrum, J. Mol. Spectrosc. 168 (1994) 455–476.

[44] M. Faye, A. L. Ven, V. Boudon, L. Manceron, P. Asselin, P. Soulard, F. K. Tchana, P. Roy, High-resolution spectroscopy of difference and combination bands of SF_6 to elucidate the $\nu_3+\nu_1-\nu_1$ and $\nu_3+\nu_2-\nu_2$ hot band structures in the ν_3 region, Mol. Phys. 112 (2014) 2504–2514.

[45] D. Papoušek, Z. Papoušková, D. P. Chong, Density functional computations of the dipole moment derivatives for halogenated methanes, J. Phys. Chem. 99 (1995) 15387–15395.

[46] S. W. Sharpe, T. J. Johnson, R. L. Sams, P. M. Chu, G. C. Rhoderick, P. A. Johnson, Gas-Phase Databases for Quantitative Infrared Spectroscopy, Appl. Spectrosc. 58 (2004) 1452–1461.

[47] M. L. Dubernet, V. Boudon, J. L. Culhane, M. S. Dimitrijevic, A. Z. Fazliez, C. Joblin, F. Kupka, G. Leto, P. L. Sidaner, P. A. Loboda, H. E. Mason, N. J. Mason, C. Mendoza, G. Mulas, T. J. Millar, L. A. Nuñez, V. I. Perevalov, N. Piskunov, Y. Ralchenko, G. Rixon, L. S. Rothman,

E. Roueff, T. A. Ryabchikova, A. Ryabtsev, S. Sahal-Bréchot, B. Schmitt, S. Schlemmer, J. Tennyson, V. G. Tyuterev, N. A. Walton, V. Wakelam, C. J. Zeippen, Virtual atomic and molecular data centre, J. Quant. Spectrosc. Radiat. Transfer 111 (2010) 2151–2159.

[48] M. L. Dubernet, B. K. Antony, Y. A. Ba, Y. L. Babikov, K. Bartschat, V. Boudon, B. J. Braams, H.-K. Chung, F. Daniel, F. Delahaye, G. D. Zanna, J. de Urquijo, A. Domaracka, M. Doronin, B. J. Drouin, M. S. Dimitrijevic, C. P. Endres, E. Quintas-Sanchez, A. Z. Fazliev, S. V. Gagarin, I. E. Gordon, U. Heiter, C. Hill, D. Jevremovic, C. Joblin, A. Kasprzak, E. Krishnakumar, G. Leto, P. A. Loboda, T. Louge, S. Maclot, B. P. Marinkovic, A. Markwick, T. Marquart, H. E. Mason, N. J. Mason, C. Mendoza, A. A. Mihajlov, T. J. Millar, N. Moreau, G. Mulas, G. Leto, Y. Pakhomov, P. Palmeri, S. Pancheshnyi, V. I. Perevalov, N. Piskunov, J. Postler, P. Gratier, P. Quinet, G. Rixon, Y. Ralchenko, Y.-J. Rhee, L. S. Rothman, E. Roueff, T. Ryabchikova, S. Sahal-Bréchot, P. Scheier, S. Schlemmer, B. Schmitt, E. Stempels, J. Tennyson, V. G. Tyuterev, V. Vujcic, V. Wakelam, N. A. Walton, O. Zatsarinny, C. J. Zeippen, C. M. Zwolf, the VAMDC Consortium, The Virtual Atomic and Molecular Data Centre (VAMDC) consortium for astrophysics, Journal of Physics B 49 (2016) 074003–1–074003–18.

[49] Y. A. Ba, C. Wenger, R. Surleau, V. Boudon, M. Rotger, L. Daumont, D. A. Bonhommeau, V. G. Tyuterev, M.-L. Dubernet, MeCaSDa and ECaSDa: Methane and ethene calculated spectroscopic databases for the virtual atomic and molecular data centre, Journal of Quantitative Spectroscopy and Radiative Transfer 130 (2013) 62–68.

Appendix A. Effective Hamiltonian parameters from the "ν_2" fit.

Table A.6 below gives the fitted values of the effective Hamiltonian parameters of CF_4 for the "ν_2" fit (see Section 4.1). Notations correspond to Equation (3). Standard deviation is given in parentheses in the unit of the last two digits.

Parameter	Polyad	Order	$\Omega(K, nC)$	$\{s\}$ C_v	$\{s'\}$ C'_v	Value / cm^{-1}	
1	GS	0	$2(0, 0A_1)$	$0000A_1$	$0000A_1$	1.9119582(35)	$\times 10^{-1}$
2	GS	2	$4(0, 0A_1)$	$0000A_1$	$0000A_1$	−6.380(33)	$\times 10^{-8}$
3	GS	2	$4(4, 0A_1)$	$0000A_1$	$0000A_1$	−3.433(17)	$\times 10^{-9}$
4	GS	4	$6(0, 0A_1)$	$0000A_1$	$0000A_1$	2.30(10)	$\times 10^{-12}$
5	GS	4	$6(4, 0A_1)$	$0000A_1$	$0000A_1$	−1.902(44)	$\times 10^{-13}$
6	GS	4	$6(6, 0A_1)$	$0000A_1$	$0000A_1$	−1.010(12)	$\times 10^{-13}$
7	GS	6	$8(0, 0A_1)$	$0000A_1$	$0000A_1$	8.544(92)	$\times 10^{-16}$
8	GS	6	$8(4, 0A_1)$	$0000A_1$	$0000A_1$	4.654(30)	$\times 10^{-17}$
9	GS	6	$8(6, 0A_1)$	$0000A_1$	$0000A_1$	−1.054(11)	$\times 10^{-17}$
10	GS	6	$8(8, 0A_1)$	$0000A_1$	$0000A_1$	4.73(45)	$\times 10^{-19}$
16	ν_2	0	$0(0, 0A_1)$	$0100E$	$0100E$	435.380220(40)	
17	ν_2	2	$2(0, 0A_1)$	$0100E$	$0100E$	−3.37820(67)	$\times 10^{-4}$
18	ν_2	2	$2(2, 0E\ )$	$0100E$	$0100E$	−1.04544(70)	$\times 10^{-4}$
19	ν_2	3	$3(3, 0A_2)$	$0100E$	$0100E$	2.9171(54)	$\times 10^{-7}$
20	ν_2	4	$4(0, 0A_1)$	$0100E$	$0100E$	7.96(32)	$\times 10^{-10}$
21	ν_2	4	$4(2, 0E\ )$	$0100E$	$0100E$	1.440(26)	$\times 10^{-9}$
22	ν_2	4	$4(4, 0A_1)$	$0100E$	$0100E$	2.681(45)	$\times 10^{-10}$
23	ν_2	4	$4(4, 0E\ )$	$0100E$	$0100E$	−1.95(14)	$\times 10^{-10}$
24	ν_2	5	$5(3, 0A_2)$	$0100E$	$0100E$	−2.270(77)	$\times 10^{-12}$
25	ν_2	6	$6(0, 0A_1)$	$0100E$	$0100E$	−7.66(36)	$\times 10^{-14}$
26	ν_2	6	$6(2, 0E\ )$	$0100E$	$0100E$	1.243(19)	$\times 10^{-13}$
28	ν_2	6	$6(4, 0E\ )$	$0100E$	$0100E$	−3.50(14)	$\times 10^{-14}$
42	ν_4	0	$0(0, 0A_1)$	$0001F_2$	$0001F_2$	631.059781(74)	
43	ν_4	1	$1(1, 0F_1)$	$0001F_2$	$0001F_2$	−2.947805(68)	$\times 10^{-1}$
44	ν_4	2	$2(0, 0A_1)$	$0001F_2$	$0001F_2$	1.0277(17)	$\times 10^{-4}$
45	ν_4	2	$2(2, 0E\ )$	$0001F_2$	$0001F_2$	−8.569(17)	$\times 10^{-5}$
46	ν_4	2	$2(2, 0F_2)$	$0001F_2$	$0001F_2$	1.7218(35)	$\times 10^{-4}$
47	ν_4	3	$3(1, 0F_1)$	$0001F_2$	$0001F_2$	−3.327(35)	$\times 10^{-7}$
48	ν_4	3	$3(3, 0F_1)$	$0001F_2$	$0001F_2$	−5.081(15)	$\times 10^{-7}$
49	ν_4	4	$4(0, 0A_1)$	$0001F_2$	$0001F_2$	−2.01(20)	$\times 10^{-9}$

Table A.6: Effective Hamiltonian parameters.

Table A.6 (continued).

Parameter	Polyad	Order	$\Omega(K, nC)$	$\{s\}$ C_v	$\{s'\}$ C'_v	Value / cm^{-1}	
50	ν_4	4	$4(2, 0E\ )$	$0001F_2$	$0001F_2$	$-3.84(23)$	$\times 10^{-9}$
51	ν_4	4	$4(2, 0F_2)$	$0001F_2$	$0001F_2$	$-3.11(26)$	$\times 10^{-9}$
52	ν_4	4	$4(4, 0A_1)$	$0001F_2$	$0001F_2$	1.177(63)	$\times 10^{-9}$
53	ν_4	4	$4(4, 0E\ )$	$0001F_2$	$0001F_2$	6.03(36)	$\times 10^{-9}$
54	ν_4	4	$4(4, 0F_2)$	$0001F_2$	$0001F_2$	4.73(26)	$\times 10^{-9}$
55	ν_4	5	$5(1, 0F_1)$	$0001F_2$	$0001F_2$	1.696(42)	$\times 10^{-11}$
56	ν_4	5	$5(3, 0F_1)$	$0001F_2$	$0001F_2$	$-2.556(75)$	$\times 10^{-11}$
57	ν_4	5	$5(5, 0F_1)$	$0001F_2$	$0001F_2$	1.106(81)	$\times 10^{-11}$
59	ν_4	6	$6(0, 0A_1)$	$0001F_2$	$0001F_2$	$-4.84(16)$	$\times 10^{-13}$
90	$2\nu_2$	2	$0(0, 0A_1)$	$0200A_1$	$0200A_1$	$-2.841606(78)$	
91	$2\nu_2$	4	$2(0, 0A_1)$	$0200A_1$	$0200A_1$	2.5371(78)	$\times 10^{-5}$
97	$2\nu_2$	4	$2(2, 0E\ )$	$0200A_1$	$0200E$	$-2.19(32)$	$\times 10^{-6}$
98	$2\nu_2$	6	$4(2, 0E\ )$	$0200A_1$	$0200E$	$-2.32(28)$	$\times 10^{-10}$
104	$2\nu_2$	2	$0(0, 0A_1)$	$0200E$	$0200E$	3.8436(17)	$\times 10^{-1}$
105	$2\nu_2$	4	$2(0, 0A_1)$	$0200E$	$0200E$	1.84(10)	$\times 10^{-6}$
119	$\nu_2 + \nu_4$	2	$0(0, 0A_1)$	$0101F_1$	$0101F_1$	2.6540(31)	$\times 10^{-1}$
120	$\nu_2 + \nu_4$	3	$1(1, 0F_1)$	$0101F_1$	$0101F_1$	5.34(17)	$\times 10^{-4}$
121	$\nu_2 + \nu_4$	4	$2(0, 0A_1)$	$0101F_1$	$0101F_1$	9.0(1.2)	$\times 10^{-6}$
146	$\nu_2 + \nu_4$	3	$1(1, 0F_1)$	$0101F_1$	$0101F_2$	$-1.754(12)$	$\times 10^{-3}$
147	$\nu_2 + \nu_4$	4	$2(2, 0E\ )$	$0101F_1$	$0101F_2$	$-7.85(69)$	$\times 10^{-6}$
148	$\nu_2 + \nu_4$	4	$2(2, 0F_2)$	$0101F_1$	$0101F_2$	$-4.41(41)$	$\times 10^{-6}$
176	$\nu_2 + \nu_4$	2	$0(0, 0A_1)$	$0101F_2$	$0101F_2$	$-3.2221(18)$	$\times 10^{-1}$
177	$\nu_2 + \nu_4$	3	$1(1, 0F_1)$	$0101F_2$	$0101F_2$	$-3.774(17)$	$\times 10^{-3}$
178	$\nu_2 + \nu_4$	4	$2(0, 0A_1)$	$0101F_2$	$0101F_2$	$-1.81(12)$	$\times 10^{-5}$
203	$\nu_3/2\nu_4$	0	$0(0, 0A_1)$	$0010F_2$	$0010F_2$	1283.236(19)	
204	$\nu_3/2\nu_4$	1	$1(1, 0F_1)$	$0010F_2$	$0010F_2$	6.4617(72)	$\times 10^{-1}$
205	$\nu_3/2\nu_4$	2	$2(0, 0A_1)$	$0010F_2$	$0010F_2$	$-6.079(36)$	$\times 10^{-4}$
206	$\nu_3/2\nu_4$	2	$2(2, 0E\ )$	$0010F_2$	$0010F_2$	1.244(13)	$\times 10^{-4}$
207	$\nu_3/2\nu_4$	2	$2(2, 0F_2)$	$0010F_2$	$0010F_2$	$-2.7521(88)$	$\times 10^{-4}$
208	$\nu_3/2\nu_4$	3	$3(1, 0F_1)$	$0010F_2$	$0010F_2$	1.787(86)	$\times 10^{-6}$

Table A.6 (continued).

Parameter	Polyad	Order	$\Omega(K, nC)$	$\{s\}$ C_v	$\{s'\}$ C'_v	Value / cm^{-1}	
209	$\nu_3/2\nu_4$	3	$3(3, 0F_1)$	$0010F_2$	$0010F_2$	9.88(97)	$\times 10^{-8}$
211	$\nu_3/2\nu_4$	4	$4(2, 0E\ )$	$0010F_2$	$0010F_2$	7.8(1.4)	$\times 10^{-9}$
212	$\nu_3/2\nu_4$	4	$4(2, 0F_2)$	$0010F_2$	$0010F_2$	−1.54(15)	$\times 10^{-8}$
213	$\nu_3/2\nu_4$	4	$4(4, 0A_1)$	$0010F_2$	$0010F_2$	7.82(69)	$\times 10^{-10}$
214	$\nu_3/2\nu_4$	4	$4(4, 0E\ )$	$0010F_2$	$0010F_2$	−1.19(23)	$\times 10^{-8}$
215	$\nu_3/2\nu_4$	4	$4(4, 0F_2)$	$0010F_2$	$0010F_2$	−1.11(16)	$\times 10^{-8}$
220	$\nu_3/2\nu_4$	6	$6(0, 0A_1)$	$0010F_2$	$0010F_2$	−4.51(12)	$\times 10^{-12}$
251	$\nu_3/2\nu_4$	3	$2(2, 0F_2)$	$0010F_2$	$0002A_1$	1.65(12)	$\times 10^{-4}$
252	$\nu_3/2\nu_4$	4	$3(3, 0F_2)$	$0010F_2$	$0002A_1$	−5.43(21)	$\times 10^{-6}$
265	$\nu_3/2\nu_4$	2	$1(1, 0F_1)$	$0010F_2$	$0002E$	−2.19(10)	$\times 10^{-2}$
266	$\nu_3/2\nu_4$	3	$2(2, 0F_2)$	$0010F_2$	$0002E$	9.30(16)	$\times 10^{-4}$
295	$\nu_3/2\nu_4$	1	$0(0, 0A_1)$	$0010F_2$	$0002F_2$	3.326(63)	
296	$\nu_3/2\nu_4$	2	$1(1, 0F_1)$	$0010F_2$	$0002F_2$	5.05(25)	$\times 10^{-2}$
297	$\nu_3/2\nu_4$	3	$2(0, 0A_1)$	$0010F_2$	$0002F_2$	6.56(12)	$\times 10^{-4}$
341	$\nu_3/2\nu_4$	2	$0(0, 0A_1)$	$0002A_1$	$0002A_1$	−2.65(19)	$\times 10^{-1}$
342	$\nu_3/2\nu_4$	4	$2(0, 0A_1)$	$0002A_1$	$0002A_1$	2.86(57)	$\times 10^{-4}$
343	$\nu_3/2\nu_4$	6	$4(0, 0A_1)$	$0002A_1$	$0002A_1$	−3.86(23)	$\times 10^{-7}$
344	$\nu_3/2\nu_4$	6	$4(4, 0A_1)$	$0002A_1$	$0002A_1$	2.59(30)	$\times 10^{-8}$
348	$\nu_3/2\nu_4$	4	$2(2, 0E\ )$	$0002A_1$	$0002E$	2.640(40)	$\times 10^{-4}$
350	$\nu_3/2\nu_4$	6	$4(4, 0E\ )$	$0002A_1$	$0002E$	5.76(27)	$\times 10^{-8}$
355	$\nu_3/2\nu_4$	4	$2(2, 0F_2)$	$0002A_1$	$0002F_2$	−4.049(82)	$\times 10^{-4}$
356	$\nu_3/2\nu_4$	5	$3(3, 0F_2)$	$0002A_1$	$0002F_2$	−6.75(42)	$\times 10^{-6}$
358	$\nu_3/2\nu_4$	6	$4(4, 0F_2)$	$0002A_1$	$0002F_2$	1.555(42)	$\times 10^{-7}$
365	$\nu_3/2\nu_4$	2	$0(0, 0A_1)$	$0002E$	$0002E$	−9.12(27)	$\times 10^{-3}$
366	$\nu_3/2\nu_4$	4	$2(0, 0A_1)$	$0002E$	$0002E$	1.387(13)	$\times 10^{-3}$
367	$\nu_3/2\nu_4$	4	$2(2, 0E\ )$	$0002E$	$0002E$	1.203(12)	$\times 10^{-3}$
380	$\nu_3/2\nu_4$	3	$1(1, 0F_1)$	$0002E$	$0002F_2$	1.525(20)	$\times 10^{-2}$
381	$\nu_3/2\nu_4$	4	$2(2, 0F_2)$	$0002E$	$0002F_2$	−7.590(84)	$\times 10^{-4}$
382	$\nu_3/2\nu_4$	5	$3(1, 0F_1)$	$0002E$	$0002F_2$	−8.20(16)	$\times 10^{-6}$
383	$\nu_3/2\nu_4$	5	$3(3, 0F_1)$	$0002E$	$0002F_2$	1.286(56)	$\times 10^{-6}$

Table A.6 (continued).

Parameter	Polyad	Order	$\Omega(K, nC)$	$\{s\}$ C_v	$\{s'\}$ C'_v	Value / cm^{-1}	
384	$\nu_3/2\nu_4$	5	$3(3, 0F_2)$	$0002E$	$0002F_2$	$-2.656(59)$	$\times 10^{-6}$
385	$\nu_3/2\nu_4$	6	$4(2, 0F_2)$	$0002E$	$0002F_2$	$-3.67(16)$	$\times 10^{-8}$
386	$\nu_3/2\nu_4$	6	$4(4, 0F_1)$	$0002E$	$0002F_2$	$-1.056(71)$	$\times 10^{-8}$
387	$\nu_3/2\nu_4$	6	$4(4, 0F_2)$	$0002E$	$0002F_2$	$-5.32(14)$	$\times 10^{-8}$
400	$\nu_3/2\nu_4$	2	$0(0, 0A_1)$	$0002F_2$	$0002F_2$	$-1.204(19)$	
401	$\nu_3/2\nu_4$	3	$1(1, 0F_1)$	$0002F_2$	$0002F_2$	$3.999(72)$	$\times 10^{-2}$
402	$\nu_3/2\nu_4$	4	$2(0, 0A_1)$	$0002F_2$	$0002F_2$	$-8.642(97)$	$\times 10^{-4}$
403	$\nu_3/2\nu_4$	4	$2(2, 0E\ )$	$0002F_2$	$0002F_2$	$1.374(14)$	$\times 10^{-3}$
404	$\nu_3/2\nu_4$	4	$2(2, 0F_2)$	$0002F_2$	$0002F_2$	$-1.1851(98)$	$\times 10^{-3}$
405	$\nu_3/2\nu_4$	5	$3(1, 0F_1)$	$0002F_2$	$0002F_2$	$-1.022(91)$	$\times 10^{-6}$
408	$\nu_3/2\nu_4$	6	$4(2, 0E\ )$	$0002F_2$	$0002F_2$	$3.41(13)$	$\times 10^{-8}$
409	$\nu_3/2\nu_4$	6	$4(2, 0F_2)$	$0002F_2$	$0002F_2$	$-2.72(13)$	$\times 10^{-8}$
410	$\nu_3/2\nu_4$	6	$4(4, 0A_1)$	$0002F_2$	$0002F_2$	$-5.56(44)$	$\times 10^{-9}$
411	$\nu_3/2\nu_4$	6	$4(4, 0E\ )$	$0002F_2$	$0002F_2$	$-4.64(16)$	$\times 10^{-8}$
412	$\nu_3/2\nu_4$	6	$4(4, 0F_2)$	$0002F_2$	$0002F_2$	$-2.72(11)$	$\times 10^{-8}$
505	$\nu_2+\nu_3/\nu_2+2\nu_4$	2	$0(0, 0A_1)$	$0110F_1$	$0110F_1$	$-2.0761(23)$	
506	$\nu_2+\nu_3/\nu_2+2\nu_4$	3	$1(1, 0F_1)$	$0110F_1$	$0110F_1$	$1.0433(72)$	$\times 10^{-2}$
507	$\nu_2+\nu_3/\nu_2+2\nu_4$	4	$2(0, 0A_1)$	$0110F_1$	$0110F_1$	$-4.72(14)$	$\times 10^{-4}$
508	$\nu_2+\nu_3/\nu_2+2\nu_4$	4	$2(2, 0E\ )$	$0110F_1$	$0110F_1$	$-3.71(11)$	$\times 10^{-4}$
509	$\nu_2+\nu_3/\nu_2+2\nu_4$	4	$2(2, 0F_2)$	$0110F_1$	$0110F_1$	$5.21(17)$	$\times 10^{-4}$
510	$\nu_2+\nu_3/\nu_2+2\nu_4$	5	$3(1, 0F_1)$	$0110F_1$	$0110F_1$	$3.8(1.0)$	$\times 10^{-7}$
511	$\nu_2+\nu_3/\nu_2+2\nu_4$	5	$3(3, 0F_1)$	$0110F_1$	$0110F_1$	$6.15(55)$	$\times 10^{-6}$
512	$\nu_2+\nu_3/\nu_2+2\nu_4$	6	$4(0, 0A_1)$	$0110F_1$	$0110F_1$	$-5.359(90)$	$\times 10^{-7}$
513	$\nu_2+\nu_3/\nu_2+2\nu_4$	6	$4(2, 0E\ )$	$0110F_1$	$0110F_1$	$4.667(62)$	$\times 10^{-7}$
514	$\nu_2+\nu_3/\nu_2+2\nu_4$	6	$4(2, 0F_2)$	$0110F_1$	$0110F_1$	$-6.523(63)$	$\times 10^{-7}$
515	$\nu_2+\nu_3/\nu_2+2\nu_4$	6	$4(4, 0A_1)$	$0110F_1$	$0110F_1$	$-5.80(26)$	$\times 10^{-8}$
516	$\nu_2+\nu_3/\nu_2+2\nu_4$	6	$4(4, 0E\ )$	$0110F_1$	$0110F_1$	$-3.701(59)$	$\times 10^{-7}$
517	$\nu_2+\nu_3/\nu_2+2\nu_4$	6	$4(4, 0F_2)$	$0110F_1$	$0110F_1$	$6.516(99)$	$\times 10^{-7}$
518	$\nu_2+\nu_3/\nu_2+2\nu_4$	7	$5(1, 0F_1)$	$0110F_1$	$0110F_1$	$1.974(85)$	$\times 10^{-9}$
519	$\nu_2+\nu_3/\nu_2+2\nu_4$	7	$5(3, 0F_1)$	$0110F_1$	$0110F_1$	$-2.595(91)$	$\times 10^{-9}$

Table A.6 (continued).

Parameter	Polyad	Order	$\Omega(K, nC)$	$\{s\}$ C_v	$\{s'\}$ C'_v	Value / cm^{-1}	
520	$\nu_2+\nu_3/\nu_2+2\nu_4$	7	$5(5,0F_1)$	$0110F_1$	$0110F_1$	6.35(49)	$\times10^{-10}$
521	$\nu_2+\nu_3/\nu_2+2\nu_4$	7	$5(5,1F_1)$	$0110F_1$	$0110F_1$	3.08(11)	$\times10^{-9}$
522	$\nu_2+\nu_3/\nu_2+2\nu_4$	8	$6(0,0A_1)$	$0110F_1$	$0110F_1$	1.068(34)	$\times10^{-10}$
523	$\nu_2+\nu_3/\nu_2+2\nu_4$	8	$6(2,0E\ )$	$0110F_1$	$0110F_1$	5.500(81)	$\times10^{-11}$
524	$\nu_2+\nu_3/\nu_2+2\nu_4$	8	$6(2,0F_2)$	$0110F_1$	$0110F_1$	−2.47(10)	$\times10^{-11}$
525	$\nu_2+\nu_3/\nu_2+2\nu_4$	8	$6(4,0A_1)$	$0110F_1$	$0110F_1$	−9.42(26)	$\times10^{-12}$
526	$\nu_2+\nu_3/\nu_2+2\nu_4$	8	$6(4,0E\ )$	$0110F_1$	$0110F_1$	−5.76(11)	$\times10^{-11}$
527	$\nu_2+\nu_3/\nu_2+2\nu_4$	8	$6(4,0F_2)$	$0110F_1$	$0110F_1$	9.79(18)	$\times10^{-11}$
528	$\nu_2+\nu_3/\nu_2+2\nu_4$	8	$6(6,0A_1)$	$0110F_1$	$0110F_1$	−1.16(12)	$\times10^{-12}$
529	$\nu_2+\nu_3/\nu_2+2\nu_4$	8	$6(6,0E\ )$	$0110F_1$	$0110F_1$	3.32(32)	$\times10^{-12}$
530	$\nu_2+\nu_3/\nu_2+2\nu_4$	8	$6(6,0F_2)$	$0110F_1$	$0110F_1$	−5.07(43)	$\times10^{-12}$
531	$\nu_2+\nu_3/\nu_2+2\nu_4$	8	$6(6,1F_2)$	$0110F_1$	$0110F_1$	−5.90(61)	$\times10^{-12}$
532	$\nu_2+\nu_3/\nu_2+2\nu_4$	3	$1(1,0F_1)$	$0110F_1$	$0110F_2$	2.306(98)	$\times10^{-3}$
533	$\nu_2+\nu_3/\nu_2+2\nu_4$	4	$2(2,0E\ )$	$0110F_1$	$0110F_2$	3.48(11)	$\times10^{-4}$
534	$\nu_2+\nu_3/\nu_2+2\nu_4$	4	$2(2,0F_2)$	$0110F_1$	$0110F_2$	2.22(16)	$\times10^{-5}$
535	$\nu_2+\nu_3/\nu_2+2\nu_4$	5	$3(1,0F_1)$	$0110F_1$	$0110F_2$	1.62(17)	$\times10^{-6}$
537	$\nu_2+\nu_3/\nu_2+2\nu_4$	5	$3(3,0F_1)$	$0110F_1$	$0110F_2$	−1.67(17)	$\times10^{-6}$
538	$\nu_2+\nu_3/\nu_2+2\nu_4$	5	$3(3,0F_2)$	$0110F_1$	$0110F_2$	1.08(21)	$\times10^{-6}$
539	$\nu_2+\nu_3/\nu_2+2\nu_4$	6	$4(2,0E\ )$	$0110F_1$	$0110F_2$	−3.556(46)	$\times10^{-7}$
540	$\nu_2+\nu_3/\nu_2+2\nu_4$	6	$4(2,0F_2)$	$0110F_1$	$0110F_2$	1.20(42)	$\times10^{-8}$
541	$\nu_2+\nu_3/\nu_2+2\nu_4$	6	$4(4,0E\ )$	$0110F_1$	$0110F_2$	2.138(30)	$\times10^{-7}$
542	$\nu_2+\nu_3/\nu_2+2\nu_4$	6	$4(4,0F_1)$	$0110F_1$	$0110F_2$	3.193(62)	$\times10^{-7}$
543	$\nu_2+\nu_3/\nu_2+2\nu_4$	6	$4(4,0F_2)$	$0110F_1$	$0110F_2$	1.42(46)	$\times10^{-8}$
544	$\nu_2+\nu_3/\nu_2+2\nu_4$	7	$5(1,0F_1)$	$0110F_1$	$0110F_2$	1.197(45)	$\times10^{-9}$
545	$\nu_2+\nu_3/\nu_2+2\nu_4$	7	$5(3,0A_2)$	$0110F_1$	$0110F_2$	1.205(26)	$\times10^{-9}$
546	$\nu_2+\nu_3/\nu_2+2\nu_4$	7	$5(3,0F_1)$	$0110F_1$	$0110F_2$	2.328(52)	$\times10^{-9}$
547	$\nu_2+\nu_3/\nu_2+2\nu_4$	7	$5(3,0F_2)$	$0110F_1$	$0110F_2$	−1.168(51)	$\times10^{-9}$
548	$\nu_2+\nu_3/\nu_2+2\nu_4$	7	$5(5,0E\ )$	$0110F_1$	$0110F_2$	1.693(51)	$\times10^{-9}$
549	$\nu_2+\nu_3/\nu_2+2\nu_4$	7	$5(5,0F_1)$	$0110F_1$	$0110F_2$	7.45(41)	$\times10^{-10}$
550	$\nu_2+\nu_3/\nu_2+2\nu_4$	7	$5(5,1F_1)$	$0110F_1$	$0110F_2$	−1.530(44)	$\times10^{-9}$

Table A.6 (continued).

Parameter	Polyad	Order	$\Omega(K,nC)$	$\{s\}$ C_v	$\{s'\}$ C'_v	Value / cm^{-1}	
551	$\nu_2+\nu_3/\nu_2+2\nu_4$	7	$5(5,0F_2)$	$0110F_1$	$0110F_2$	1.490(55)	$\times10^{-9}$
552	$\nu_2+\nu_3/\nu_2+2\nu_4$	8	$6(2,0E\ )$	$0110F_1$	$0110F_2$	−3.729(66)	$\times10^{-11}$
553	$\nu_2+\nu_3/\nu_2+2\nu_4$	8	$6(2,0F_2)$	$0110F_1$	$0110F_2$	1.506(95)	$\times10^{-11}$
555	$\nu_2+\nu_3/\nu_2+2\nu_4$	8	$6(4,0F_1)$	$0110F_1$	$0110F_2$	1.374(41)	$\times10^{-11}$
556	$\nu_2+\nu_3/\nu_2+2\nu_4$	8	$6(4,0F_2)$	$0110F_1$	$0110F_2$	−1.352(55)	$\times10^{-11}$
557	$\nu_2+\nu_3/\nu_2+2\nu_4$	8	$6(6,0A_2)$	$0110F_1$	$0110F_2$	−2.65(22)	$\times10^{-12}$
562	$\nu_2+\nu_3/\nu_2+2\nu_4$	2	$0(0,0A_1)$	$0110F_2$	$0110F_2$	−2.4859(24)	
563	$\nu_2+\nu_3/\nu_2+2\nu_4$	3	$1(1,0F_1)$	$0110F_2$	$0110F_2$	1.6860(93)	$\times10^{-2}$
564	$\nu_2+\nu_3/\nu_2+2\nu_4$	4	$2(0,0A_1)$	$0110F_2$	$0110F_2$	4.90(14)	$\times10^{-4}$
565	$\nu_2+\nu_3/\nu_2+2\nu_4$	4	$2(2,0E\ )$	$0110F_2$	$0110F_2$	3.96(13)	$\times10^{-4}$
566	$\nu_2+\nu_3/\nu_2+2\nu_4$	4	$2(2,0F_2)$	$0110F_2$	$0110F_2$	−6.87(17)	$\times10^{-4}$
567	$\nu_2+\nu_3/\nu_2+2\nu_4$	5	$3(1,0F_1)$	$0110F_2$	$0110F_2$	−5.78(50)	$\times10^{-6}$
569	$\nu_2+\nu_3/\nu_2+2\nu_4$	6	$4(0,0A_1)$	$0110F_2$	$0110F_2$	3.885(98)	$\times10^{-7}$
570	$\nu_2+\nu_3/\nu_2+2\nu_4$	6	$4(2,0E\ )$	$0110F_2$	$0110F_2$	−2.427(50)	$\times10^{-7}$
571	$\nu_2+\nu_3/\nu_2+2\nu_4$	6	$4(2,0F_2)$	$0110F_2$	$0110F_2$	9.748(88)	$\times10^{-7}$
572	$\nu_2+\nu_3/\nu_2+2\nu_4$	6	$4(4,0A_1)$	$0110F_2$	$0110F_2$	7.03(29)	$\times10^{-8}$
573	$\nu_2+\nu_3/\nu_2+2\nu_4$	6	$4(4,0E\ )$	$0110F_2$	$0110F_2$	2.86(49)	$\times10^{-8}$
574	$\nu_2+\nu_3/\nu_2+2\nu_4$	6	$4(4,0F_2)$	$0110F_2$	$0110F_2$	−3.191(57)	$\times10^{-7}$
575	$\nu_2+\nu_3/\nu_2+2\nu_4$	7	$5(1,0F_1)$	$0110F_2$	$0110F_2$	2.314(56)	$\times10^{-9}$
576	$\nu_2+\nu_3/\nu_2+2\nu_4$	7	$5(3,0F_1)$	$0110F_2$	$0110F_2$	−9.64(51)	$\times10^{-10}$
577	$\nu_2+\nu_3/\nu_2+2\nu_4$	7	$5(5,0F_1)$	$0110F_2$	$0110F_2$	1.295(35)	$\times10^{-9}$
578	$\nu_2+\nu_3/\nu_2+2\nu_4$	7	$5(5,1F_1)$	$0110F_2$	$0110F_2$	8.04(50)	$\times10^{-10}$
579	$\nu_2+\nu_3/\nu_2+2\nu_4$	8	$6(0,0A_1)$	$0110F_2$	$0110F_2$	−1.279(19)	$\times10^{-10}$
580	$\nu_2+\nu_3/\nu_2+2\nu_4$	8	$6(2,0E\ )$	$0110F_2$	$0110F_2$	−2.142(30)	$\times10^{-11}$
581	$\nu_2+\nu_3/\nu_2+2\nu_4$	8	$6(2,0F_2)$	$0110F_2$	$0110F_2$	1.0103(91)	$\times10^{-10}$
603	$\nu_2+\nu_3/\nu_2+2\nu_4$	4	$1(1,0F_1)$	$0110F_1$	$0102A_1$	2.63(11)	$\times10^{-2}$
611	$\nu_2+\nu_3/\nu_2+2\nu_4$	5	$2(2,0F_2)$	$0110F_1$	$0102A_2$	−9.93(25)	$\times10^{-4}$
674	$\nu_2+\nu_3/\nu_2+2\nu_4$	5	$2(2,0F_2)$	$0110F_2$	$0102E$	−2.468(45)	$\times10^{-3}$
693	$\nu_2+\nu_3/\nu_2+2\nu_4$	4	$1(1,0F_1)$	$0110F_2$	$0102A_2$	1.84(15)	$\times10^{-2}$
701	$\nu_2+\nu_3/\nu_2+2\nu_4$	4	$1(1,0F_1)$	$0110F_2$	$0102E$	3.48(11)	$\times10^{-2}$

650

Table A.6 (continued).

Parameter	Polyad	Order	$\Omega(K, nC)$	$\{s\}$ C_v	$\{s'\}$ C'_v	Value / cm^{-1}	
757	$\nu_2+\nu_3/\nu_2+2\nu_4$	4	$0(0,0A_1)$	$0102E$	$0102E$	2.253(51)	
771	$\nu_2+\nu_3/\nu_2+2\nu_4$	4	$0(0,0A_1)$	$0102E$	$0102E$	3.79(48)	$\times10^{-1}$
779	$\nu_2+\nu_3/\nu_2+2\nu_4$	5	$1(1,0F_1)$	$0102E$	$0102F_1$	−5.64(32)	$\times10^{-2}$
787	$\nu_2+\nu_3/\nu_2+2\nu_4$	5	$1(1,0F_1)$	$0102E$	$0102F_2$	−8.03(28)	$\times10^{-2}$
795	$\nu_2+\nu_3/\nu_2+2\nu_4$	4	$0(0,0A_1)$	$0102A_1$	$0102A_1$	4.61(23)	$\times10^{-1}$
796	$\nu_2+\nu_3/\nu_2+2\nu_4$	6	$2(0,0A_1)$	$0102A_1$	$0102A_1$	−1.879(33)	$\times10^{-3}$
811	$\nu_2+\nu_3/\nu_2+2\nu_4$	4	$0(0,0A_1)$	$0102A_2$	$0102A_2$	−6.78(32)	$\times10^{-1}$
815	$\nu_2+\nu_3/\nu_2+2\nu_4$	6	$2(2,0E\ )$	$0102A_2$	$0102E$	−6.408(79)	$\times10^{-4}$
826	$\nu_2+\nu_3/\nu_2+2\nu_4$	4	$0(0,0A_1)$	$0102E$	$0102E$	−2.913(72)	$\times10^{-1}$
834	$\nu_2+\nu_3/\nu_2+2\nu_4$	5	$1(1,0F_1)$	$0102E$	$0102F_1$	−3.026(62)	$\times10^{-2}$
842	$\nu_2+\nu_3/\nu_2+2\nu_4$	5	$1(1,0F_1)$	$0102E$	$0102F_2$	−1.296(78)	$\times10^{-2}$
850	$\nu_2+\nu_3/\nu_2+2\nu_4$	4	$0(0,0A_1)$	$0102F_1$	$0102F_1$	6.579(60)	$\times10^{-1}$
851	$\nu_2+\nu_3/\nu_2+2\nu_4$	5	$1(1,0F_1)$	$0102F_1$	$0102F_1$	−3.06(11)	$\times10^{-2}$
863	$\nu_2+\nu_3/\nu_2+2\nu_4$	5	$1(1,0F_1)$	$0102F_1$	$0102F_2$	−2.973(56)	$\times10^{-2}$
875	$\nu_2+\nu_3/\nu_2+2\nu_4$	4	$0(0,0A_1)$	$0102F_2$	$0102F_2$	−8.5(1.1)	$\times10^{-2}$
876	$\nu_2+\nu_3/\nu_2+2\nu_4$	5	$1(1,0F_1)$	$0102F_2$	$0102F_2$	4.66(11)	$\times10^{-2}$
877	$\nu_2+\nu_3/\nu_2+2\nu_4$	6	$2(0,0A_1)$	$0102F_2$	$0102F_2$	5.66(26)	$\times10^{-4}$

Appendix B. Effective Hamiltonian parameters from the "ν_1" fit.

Table B.7 below gives the fitted values of the effective Hamiltonian parameters of CF_4 for the "ν_1" fit (see Section 4.2). Notations correspond to Equation (3). Standard deviation is given in parentheses in the unit of the last two digits.

Parameter	Polyad	Order	$\Omega(K, nC)$	$\{s\}$ C_v	$\{s'\}$ C'_v	Value / cm^{-1}	
64	ν_1	0	$0(0, 0A_1)$	$1000A_1$	$1000A_1$	909.072146(52)	
65	ν_1	2	$2(0, 0A_1)$	$1000A_1$	$1000A_1$	−3.47048(68)	$\times 10^{-4}$
66	ν_1	4	$4(0, 0A_1)$	$1000A_1$	$1000A_1$	−2.65(30)	$\times 10^{-10}$
67	ν_1	4	$4(4, 0A_1)$	$1000A_1$	$1000A_1$	−1.31(30)	$\times 10^{-11}$
68	ν_1	6	$6(0, 0A_1)$	$1000A_1$	$1000A_1$	6.51(38)	$\times 10^{-14}$
69	ν_1	6	$6(4, 0A_1)$	$1000A_1$	$1000A_1$	−5.47(28)	$\times 10^{-15}$
70	ν_1	6	$6(6, 0A_1)$	$1000A_1$	$1000A_1$	1.186(74)	$\times 10^{-15}$
299	$\nu_1 + \nu_4$	2	$0(0, 0A_1)$	$1001F_2$	$1001F_2$	−6.7356(23)	$\times 10^{-1}$
300	$\nu_1 + \nu_4$	3	$1(1, 0F_1)$	$1001F_2$	$1001F_2$	6.547(31)	$\times 10^{-3}$
301	$\nu_1 + \nu_4$	4	$2(0, 0A_1)$	$1001F_2$	$1001F_2$	−7.0(1.2)	$\times 10^{-6}$
302	$\nu_1 + \nu_4$	4	$2(2, 0E\ )$	$1001F_2$	$1001F_2$	1.31(17)	$\times 10^{-5}$
303	$\nu_1 + \nu_4$	4	$2(2, 0F_2)$	$1001F_2$	$1001F_2$	2.25(25)	$\times 10^{-5}$
304	$\nu_1 + \nu_4$	5	$3(1, 0F_1)$	$1001F_2$	$1001F_2$	1.49(24)	$\times 10^{-7}$
305	$\nu_1 + \nu_4$	5	$3(3, 0F_1)$	$1001F_2$	$1001F_2$	2.78(14)	$\times 10^{-7}$
306	$\nu_1 + \nu_4$	6	$4(0, 0A_1)$	$1001F_2$	$1001F_2$	1.86(18)	$\times 10^{-8}$
307	$\nu_1 + \nu_4$	6	$4(2, 0E\ )$	$1001F_2$	$1001F_2$	4.96(19)	$\times 10^{-8}$
308	$\nu_1 + \nu_4$	6	$4(2, 0F_2)$	$1001F_2$	$1001F_2$	−1.55(29)	$\times 10^{-8}$
309	$\nu_1 + \nu_4$	6	$4(4, 0A_1)$	$1001F_2$	$1001F_2$	−1.83(17)	$\times 10^{-9}$
310	$\nu_1 + \nu_4$	6	$4(4, 0E\ )$	$1001F_2$	$1001F_2$	−6.29(27)	$\times 10^{-8}$
311	$\nu_1 + \nu_4$	6	$4(4, 0F_2)$	$1001F_2$	$1001F_2$	−4.87(20)	$\times 10^{-8}$
312	$\nu_1 + \nu_4$	7	$5(1, 0F_1)$	$1001F_2$	$1001F_2$	3.55(43)	$\times 10^{-11}$
313	$\nu_1 + \nu_4$	7	$5(3, 0F_1)$	$1001F_2$	$1001F_2$	3.29(42)	$\times 10^{-11}$
315	$\nu_1 + \nu_4$	7	$5(5, 1F_1)$	$1001F_2$	$1001F_2$	−1.43(19)	$\times 10^{-11}$
316	$\nu_1 + \nu_4$	8	$6(0, 0A_1)$	$1001F_2$	$1001F_2$	−1.143(82)	$\times 10^{-11}$
317	$\nu_1 + \nu_4$	8	$6(2, 0E\ )$	$1001F_2$	$1001F_2$	1.372(26)	$\times 10^{-11}$
318	$\nu_1 + \nu_4$	8	$6(2, 0F_2)$	$1001F_2$	$1001F_2$	−5.30(60)	$\times 10^{-12}$
320	$\nu_1 + \nu_4$	8	$6(4, 0E\ )$	$1001F_2$	$1001F_2$	−2.337(46)	$\times 10^{-11}$
321	$\nu_1 + \nu_4$	8	$6(4, 0F_2)$	$1001F_2$	$1001F_2$	−1.320(61)	$\times 10^{-11}$
322	$\nu_1 + \nu_4$	8	$6(6, 0A_1)$	$1001F_2$	$1001F_2$	−6.82(85)	$\times 10^{-13}$
323	$\nu_1 + \nu_4$	8	$6(6, 0E\ )$	$1001F_2$	$1001F_2$	4.47(18)	$\times 10^{-12}$

Table B.7: Effective Hamiltonian parameters.

Table B.7 (continued).

Parameter	Polyad	Order	$\Omega(K, nC)$	$\{s\}$ C_v	$\{s'\}$ C'_v	Value / cm^{-1}	
325	$\nu_1 + \nu_4$	8	$6(6, 1F_2)$	$1001F_2$	$1001F_2$	5.99(24)	$\times 10^{-12}$
326	$2\nu_1/\nu_3 + \nu_4$	2	$0(0, 0A_1)$	$2000A_1$	$2000A_1$	−2.328912(48)	
327	$2\nu_1/\nu_3 + \nu_4$	4	$2(0, 0A_1)$	$2000A_1$	$2000A_1$	−3.252(20)	$\times 10^{-6}$
329	$2\nu_1/\nu_3 + \nu_4$	6	$4(4, 0A_1)$	$2000A_1$	$2000A_1$	−1.82(16)	$\times 10^{-11}$
540	$\nu_2 + \nu_3/\nu_2 + 2\nu_4$	2	$0(0, 0A_1)$	$1010F_2$	$1010F_2$	−7.268(32)	
541	$\nu_2 + \nu_3/\nu_2 + 2\nu_4$	3	$1(1, 0F_1)$	$1010F_2$	$1010F_2$	2.54(12)	$\times 10^{-2}$
542	$\nu_2 + \nu_3/\nu_2 + 2\nu_4$	4	$2(0, 0A_1)$	$1010F_2$	$1010F_2$	1.03(14)	$\times 10^{-4}$
543	$\nu_2 + \nu_3/\nu_2 + 2\nu_4$	4	$2(2, 0E\ )$	$1010F_2$	$1010F_2$	−1.068(14)	$\times 10^{-3}$
544	$\nu_2 + \nu_3/\nu_2 + 2\nu_4$	4	$2(2, 0F_2)$	$1010F_2$	$1010F_2$	−1.79(20)	$\times 10^{-4}$
545	$\nu_2 + \nu_3/\nu_2 + 2\nu_4$	5	$3(1, 0F_1)$	$1010F_2$	$1010F_2$	−1.358(33)	$\times 10^{-5}$
546	$\nu_2 + \nu_3/\nu_2 + 2\nu_4$	5	$3(3, 0F_1)$	$1010F_2$	$1010F_2$	1.775(27)	$\times 10^{-5}$
547	$\nu_2 + \nu_3/\nu_2 + 2\nu_4$	6	$4(0, 0A_1)$	$1010F_2$	$1010F_2$	−3.591(66)	$\times 10^{-7}$
550	$\nu_2 + \nu_3/\nu_2 + 2\nu_4$	6	$4(4, 0A_1)$	$1010F_2$	$1010F_2$	−2.11(11)	$\times 10^{-8}$
552	$\nu_2 + \nu_3/\nu_2 + 2\nu_4$	6	$4(4, 0F_2)$	$1010F_2$	$1010F_2$	5.99(24)	$\times 10^{-8}$
553	$\nu_2 + \nu_3/\nu_2 + 2\nu_4$	7	$5(1, 0F_1)$	$1010F_2$	$1010F_2$	−9.85(45)	$\times 10^{-10}$
554	$\nu_2 + \nu_3/\nu_2 + 2\nu_4$	7	$5(3, 0F_1)$	$1010F_2$	$1010F_2$	9.26(43)	$\times 10^{-10}$
556	$\nu_2 + \nu_3/\nu_2 + 2\nu_4$	7	$5(5, 1F_1)$	$1010F_2$	$1010F_2$	−2.273(62)	$\times 10^{-9}$
557	$\nu_2 + \nu_3/\nu_2 + 2\nu_4$	8	$6(0, 0A_1)$	$1010F_2$	$1010F_2$	−4.50(15)	$\times 10^{-11}$
567	$\nu_2 + \nu_3/\nu_2 + 2\nu_4$	5	$2(2, 0F_2)$	$1010F_2$	$1002A_1$	−1.451(30)	$\times 10^{-3}$
568	$\nu_2 + \nu_3/\nu_2 + 2\nu_4$	6	$3(3, 0F_2)$	$1010F_2$	$1002A_1$	2.199(38)	$\times 10^{-5}$
569	$\nu_2 + \nu_3/\nu_2 + 2\nu_4$	7	$4(2, 0F_2)$	$1010F_2$	$1002A_1$	2.122(48)	$\times 10^{-7}$
573	$\nu_2 + \nu_3/\nu_2 + 2\nu_4$	4	$1(1, 0F_1)$	$1010F_2$	$1002E$	−1.205(21)	$\times 10^{-1}$
574	$\nu_2 + \nu_3/\nu_2 + 2\nu_4$	5	$2(2, 0F_2)$	$1010F_2$	$1002E$	−1.692(36)	$\times 10^{-3}$
575	$\nu_2 + \nu_3/\nu_2 + 2\nu_4$	6	$3(1, 0F_1)$	$1010F_2$	$1002E$	−1.313(29)	$\times 10^{-5}$
579	$\nu_2 + \nu_3/\nu_2 + 2\nu_4$	7	$4(4, 0F_1)$	$1010F_2$	$1002E$	−1.14(39)	$\times 10^{-8}$
580	$\nu_2 + \nu_3/\nu_2 + 2\nu_4$	7	$4(4, 0F_2)$	$1010F_2$	$1002E$	−9.22(22)	$\times 10^{-8}$
587	$\nu_2 + \nu_3/\nu_2 + 2\nu_4$	3	$0(0, 0A_1)$	$1010F_2$	$1002F_2$	2.259(43)	
588	$\nu_2 + \nu_3/\nu_2 + 2\nu_4$	4	$1(1, 0F_1)$	$1010F_2$	$1002F_2$	−4.52(16)	$\times 10^{-2}$
589	$\nu_2 + \nu_3/\nu_2 + 2\nu_4$	5	$2(0, 0A_1)$	$1010F_2$	$1002F_2$	−1.401(23)	$\times 10^{-3}$
590	$\nu_2 + \nu_3/\nu_2 + 2\nu_4$	5	$2(2, 0E\ )$	$1010F_2$	$1002F_2$	2.480(35)	$\times 10^{-3}$

Table B.7 (continued).

Parameter	Polyad	Order	$\Omega(K, nC)$	$\{s\}$ C_v	$\{s'\}$ C'_v	Value / cm^{-1}	
591	$\nu_2+\nu_3/\nu_2+2\nu_4$	5	$2(2,0F_2)$	$1010F_2$	$1002F_2$	$-7.94(33)$	$\times10^{-4}$
592	$\nu_2+\nu_3/\nu_2+2\nu_4$	6	$3(1,0F_1)$	$1010F_2$	$1002F_2$	$1.717(53)$	$\times10^{-5}$
593	$\nu_2+\nu_3/\nu_2+2\nu_4$	6	$3(3,0F_1)$	$1010F_2$	$1002F_2$	$-1.957(31)$	$\times10^{-5}$
594	$\nu_2+\nu_3/\nu_2+2\nu_4$	6	$3(3,0F_2)$	$1010F_2$	$1002F_2$	$-3.544(68)$	$\times10^{-5}$
595	$\nu_2+\nu_3/\nu_2+2\nu_4$	7	$4(0,0A_1)$	$1010F_2$	$1002F_2$	$4.305(67)$	$\times10^{-7}$
596	$\nu_2+\nu_3/\nu_2+2\nu_4$	7	$4(2,0E\ )$	$1010F_2$	$1002F_2$	$2.412(41)$	$\times10^{-7}$
598	$\nu_2+\nu_3/\nu_2+2\nu_4$	7	$4(4,0A_1)$	$1010F_2$	$1002F_2$	$-2.49(23)$	$\times10^{-8}$
599	$\nu_2+\nu_3/\nu_2+2\nu_4$	7	$4(4,0E\ )$	$1010F_2$	$1002F_2$	$-7.08(30)$	$\times10^{-8}$
600	$\nu_2+\nu_3/\nu_2+2\nu_4$	7	$4(4,0F_1)$	$1010F_2$	$1002F_2$	$-6.44(26)$	$\times10^{-8}$
602	$\nu_2+\nu_3/\nu_2+2\nu_4$	8	$5(1,0F_1)$	$1010F_2$	$1002F_2$	$2.459(55)$	$\times10^{-9}$
603	$\nu_2+\nu_3/\nu_2+2\nu_4$	8	$5(3,0F_1)$	$1010F_2$	$1002F_2$	$-3.061(67)$	$\times10^{-9}$
604	$\nu_2+\nu_3/\nu_2+2\nu_4$	8	$5(3,0F_2)$	$1010F_2$	$1002F_2$	$9.47(88)$	$\times10^{-10}$
606	$\nu_2+\nu_3/\nu_2+2\nu_4$	8	$5(5,0F_1)$	$1010F_2$	$1002F_2$	$1.627(43)$	$\times10^{-9}$
607	$\nu_2+\nu_3/\nu_2+2\nu_4$	8	$5(5,1F_1)$	$1010F_2$	$1002F_2$	$9.73(36)$	$\times10^{-10}$
608	$\nu_2+\nu_3/\nu_2+2\nu_4$	8	$5(5,0F_2)$	$1010F_2$	$1002F_2$	$1.110(30)$	$\times10^{-9}$
609	$\nu_2+\nu_3/\nu_2+2\nu_4$	4	$0(0,0A_1)$	$1002A_1$	$1002A_1$	$7.4(1.9)$	$\times10^{-1}$
610	$\nu_2+\nu_3/\nu_2+2\nu_4$	6	$2(0,0A_1)$	$1002A_1$	$1002A_1$	$6.50(24)$	$\times10^{-3}$
611	$\nu_2+\nu_3/\nu_2+2\nu_4$	8	$4(0,0A_1)$	$1002A_1$	$1002A_1$	$-2.915(79)$	$\times10^{-6}$
613	$\nu_2+\nu_3/\nu_2+2\nu_4$	6	$2(2,0E\ )$	$1002A_1$	$1002E$	$-2.50(20)$	$\times10^{-4}$
614	$\nu_2+\nu_3/\nu_2+2\nu_4$	8	$4(2,0E\ )$	$1002A_1$	$1002E$	$-1.139(52)$	$\times10^{-7}$
615	$\nu_2+\nu_3/\nu_2+2\nu_4$	8	$4(4,0E\ )$	$1002A_1$	$1002E$	$1.228(27)$	$\times10^{-7}$
616	$\nu_2+\nu_3/\nu_2+2\nu_4$	6	$2(2,0F_2)$	$1002A_1$	$1002F_2$	$-1.367(42)$	$\times10^{-3}$
617	$\nu_2+\nu_3/\nu_2+2\nu_4$	7	$3(3,0F_2)$	$1002A_1$	$1002F_2$	$-1.495(44)$	$\times10^{-5}$
618	$\nu_2+\nu_3/\nu_2+2\nu_4$	8	$4(2,0F_2)$	$1002A_1$	$1002F_2$	$-3.817(99)$	$\times10^{-7}$
619	$\nu_2+\nu_3/\nu_2+2\nu_4$	8	$4(4,0F_2)$	$1002A_1$	$1002F_2$	$2.928(29)$	$\times10^{-7}$
620	$\nu_2+\nu_3/\nu_2+2\nu_4$	4	$0(0,0A_1)$	$1002E$	$1002E$	$-3.15(21)$	$\times10^{-2}$
621	$\nu_2+\nu_3/\nu_2+2\nu_4$	6	$2(0,0A_1)$	$1002E$	$1002E$	$2.36(17)$	$\times10^{-4}$
622	$\nu_2+\nu_3/\nu_2+2\nu_4$	6	$2(2,0E\ )$	$1002E$	$1002E$	$1.472(22)$	$\times10^{-3}$
623	$\nu_2+\nu_3/\nu_2+2\nu_4$	7	$3(3,0A_2)$	$1002E$	$1002E$	$2.76(23)$	$\times10^{-6}$
625	$\nu_2+\nu_3/\nu_2+2\nu_4$	8	$4(2,0E\ )$	$1002E$	$1002E$	$2.89(38)$	$\times10^{-8}$

Table B.7 (continued).

Parameter	Polyad	Order	$\Omega(K, nC)$	$\{s\}$ C_v	$\{s'\}$ C'_v	Value / cm^{-1}	
626	$\nu_2+\nu_3/\nu_2+2\nu_4$	8	$4(4,0A_1)$	$1002E$	$1002E$	4.08(15)	$\times10^{-8}$
627	$\nu_2+\nu_3/\nu_2+2\nu_4$	8	$4(4,0E\ )$	$1002E$	$1002E$	−4.135(29)	$\times10^{-7}$
628	$\nu_2+\nu_3/\nu_2+2\nu_4$	5	$1(1,0F_1)$	$1002E$	$1002F_2$	−5.35(11)	$\times10^{-2}$
629	$\nu_2+\nu_3/\nu_2+2\nu_4$	6	$2(2,0F_2)$	$1002E$	$1002F_2$	−3.61(18)	$\times10^{-4}$
630	$\nu_2+\nu_3/\nu_2+2\nu_4$	7	$3(1,0F_1)$	$1002E$	$1002F_2$	−1.741(26)	$\times10^{-5}$
631	$\nu_2+\nu_3/\nu_2+2\nu_4$	7	$3(3,0F_1)$	$1002E$	$1002F_2$	2.512(22)	$\times10^{-5}$
632	$\nu_2+\nu_3/\nu_2+2\nu_4$	7	$3(3,0F_2)$	$1002E$	$1002F_2$	−1.248(27)	$\times10^{-5}$
633	$\nu_2+\nu_3/\nu_2+2\nu_4$	8	$4(2,0F_2)$	$1002E$	$1002F_2$	1.136(33)	$\times10^{-7}$
634	$\nu_2+\nu_3/\nu_2+2\nu_4$	8	$4(4,0F_1)$	$1002E$	$1002F_2$	3.048(27)	$\times10^{-7}$
635	$\nu_2+\nu_3/\nu_2+2\nu_4$	8	$4(4,0F_2)$	$1002E$	$1002F_2$	9.13(35)	$\times10^{-8}$
636	$\nu_2+\nu_3/\nu_2+2\nu_4$	4	$0(0,0A_1)$	$1002F_2$	$1002F_2$	1.243(32)	
637	$\nu_2+\nu_3/\nu_2+2\nu_4$	5	$1(1,0F_1)$	$1002F_2$	$1002F_2$	−3.38(12)	$\times10^{-2}$
638	$\nu_2+\nu_3/\nu_2+2\nu_4$	6	$2(0,0A_1)$	$1002F_2$	$1002F_2$	−8.03(15)	$\times10^{-4}$
639	$\nu_2+\nu_3/\nu_2+2\nu_4$	6	$2(2,0E\ )$	$1002F_2$	$1002F_2$	2.118(18)	$\times10^{-3}$
640	$\nu_2+\nu_3/\nu_2+2\nu_4$	6	$2(2,0F_2)$	$1002F_2$	$1002F_2$	−3.82(26)	$\times10^{-4}$
641	$\nu_2+\nu_3/\nu_2+2\nu_4$	7	$3(1,0F_1)$	$1002F_2$	$1002F_2$	5.23(34)	$\times10^{-6}$
645	$\nu_2+\nu_3/\nu_2+2\nu_4$	8	$4(2,0F_2)$	$1002F_2$	$1002F_2$	−5.002(49)	$\times10^{-7}$